REPORT DOCUMENTATION PAGE

1a. REPORT SECURITY CLASSIFICATION Unclassified	1b. RESTRICTIVE MARKINGS None
2a. SECURITY CLASSIFICATION AUTHORITY	3. DISTRIBUTION / AVAILABILITY OF REPORT Approved for Public Release; Distribution Unlimited
2b. DECLASSIFICATION / DOWNGRADING SCHEDULE	
4. PERFORMING ORGANIZATION REPORT NUMBER(S) Final Report WII-9942-01-TR-01	5. MONITORING ORGANIZATION REPORT NUMBER(S) None
6a. NAME OF PERFORMING ORGANIZATION Winzen International, Inc. 6b. OFFICE SYMBOL (*If applicable*)	7a. NAME OF MONITORING ORGANIZATION U.S. Army Missile Command
6c. ADDRESS (*City, State, and ZIP Code*) 12001 Network Blvd., Suite 200 San Antonio, Texas 78249	7b. ADDRESS (*City, State, and ZIP Code*) Attn: AMSMI-RD-DP-TT Redstone Arsenal, AL 35898-5244
8a. NAME OF FUNDING / SPONSORING ORGANIZATION Defense Advanced Research Projects Agency 8b. OFFICE SYMBOL (*If applicable*) PMO/SBIR	9. PROCUREMENT INSTRUMENT IDENTIFICATION NUMBER Contract No. DAAH01-88-C-0715
8c. ADDRESS (*City, State, and ZIP Code*) 1400 Wilson Blvd. Arlington, VA 22209-2308	10. SOURCE OF FUNDING NUMBERS PROGRAM ELEMENT NO.

19960614 003

11. TITLE (*Include Security Classification*)
Long Duration Balloon Technology Survey (u)

12. PERSONAL AUTHOR(S)
Scott, P.G., Lew, T.M., Wilbeck, J.S., Rand, J.L., Brezinsky, R.H.

13a. TYPE OF REPORT	13b. TIME COVERED	14. DATE OF REPORT (*Year, Month, Day*)	15. PAGE COUNT
Final	FROM 8/11/88 TO 2/28/89	89-3-11	66 Pages

16. SUPPLEMENTARY NOTATION

17. COSATI CODES			18. SUBJECT TERMS (*Continue on reverse if necessary and identify by block number*)
FIELD	GROUP	SUB-GROUP	superpressure balloon, balloon, biaxially oriented Nylon, long duration balloon
01	03	11	

19. ABSTRACT (*Continue on reverse if necessary and identify by block number*)

This feasibility study addresses the design and fabrication of a long endurance balloon-vehicle capable of supporting 50 pounds at 120,000 feet for up to one year. The concept makes use of the experience gained by the scientific community over the past two decades in flying smaller payloads for long periods of time. The result of the effort is a prototype balloon which has a better lift to weight ratio than previous designs. This was achieved by the use of a novel shape (multiple intersecting spheres) and the use of a material new in the area of ballooning (Emblem®, a biaxially oriented Nylon 6). This film demonstrates very high strength without displaying the susceptibility of prior films to pinholing. Other results of the effort are two analytical tools and specialized fabrication techniques. The analytical tools are a heat transfer model for predicting maximum and minimum supertemperatures of the balloon gas, and mechanical model to design the superpressure balloons for particular flight scenarios.

20. DISTRIBUTION / AVAILABILITY OF ABSTRACT	21. ABSTRACT SECURITY CLASSIFICATION	
☒ UNCLASSIFIED/UNLIMITED ☐ SAME AS RPT. ☐ DTIC USERS	Unlimited	
22a. NAME OF RESPONSIBLE INDIVIDUAL Dr. Ralph Norman	22b. TELEPHONE (*Include Area Code*) (205) 876-2541	22c. OFFICE SYMBOL AMSMI-RD-DP-TT

DD FORM 1473, 84 MAR 83 APR edition may be used until exhausted. All other editions are obsolete.

UNABLE TO GET PAGE 3-4 BECAUSE THIS REPORT

IS OUT OF PRINT, PER JERRY HAGOOD (205 876-3700)

OF U. S. ARMY MISSILE COMMAND, REDSTONE

ARSENAL, AL.

JULY 2, 1996

PROJECT SUMMARY

A number of DoD studies are currently being conducted which use high altitude, free floating balloon platforms to support communications and surveillance efforts. Compared to a satellite based system, the long duration balloon based system represents an extremely economical and rapidly deployable system. During times of conflict, the high operational altitudes combined with negligible observability also make a balloon-based system difficult to detect and destroy.

Using current balloon designs, float durations are limited to only a few days. The development of a long duration balloon platform is contingent upon the development of a superpressure balloon system. Unique characteristics of the superpressure balloon are that it maintains constant volume and that it does not vent lift gas. Maintaining constant volume allows the superpressure balloon to maintain a nominally constant altitude without the use of ballast. Combined with the fact that gas is not vented, this characteristic gives the superpressure balloon the potential for very long duration flight. The overall objective of this Phase I effort was to demonstrate technical feasibility of producing a reliable constant volume balloon platform capable of supporting a 50 pound payload at 120,000 feet for one year.

During the Phase I effort, two analytical models were developed. One was a thermal model of the superpressure balloon which was used to predict the maximum and minimum supertemperatures of the lift gas. The prediction of supertemperatures is critical to the balloon design for two reasons. First of all, the maximum supertemperature determines maximum expected superpressure in the balloon material (wall). This determines the maximum stress levels for which the balloon must be designed. Secondly, the minimum supertemperature determines the amount of gas in the balloon necessary to prevent loss of volume because of loss of pressure. The thermal model was also used in the material selection task. By allowing a comparison of the thermal effects of different balloon materials, the model helped to optimize the choice of balloon material.

A balloon design study was conducted to determine the optimum shape for a superpressure balloon. Tradeoff studies were conducted to minimize balloon weight and fabrication complexity. Model balloons were then fabricated and burst tested.

The results of this Phase I effort clearly demonstrated the technical feasibility of developing a reliable superpressure balloon platform capable of supporting 50 pounds at 120,000 feet for extended periods. There were no insurmountable technical obstacles identified in Phase I. The prototype balloon developed in Phase I has a much better lift to weight ratio than previous designs. This was achieved by the use of a novel shape (multiple intersecting spheres) and the use of a material new in the area of ballooning (a biaxially oriented Nylon 6). This film demonstrates very high strength without displaying the susceptibility of prior films to pinholing. An adhesive tape was also developed which should allow for the development of simple but rapid fabrication techniques.

PREFACE

This report documents the research program conducted by Winzen International, Inc. (WII) in support of the Small Business Innovative Reasearch (SBIR) Program from August 11, 1988 through February 28, 1989. The work was performed under sponsorship of the Defense Advanced Research Projects Agency (DARPA), ARPA Order No. 5916, Amendment 9. The issuing agency was the U.S. Army Missile Command, Contract No. DAAH01-88-C-0715. Dr. Ralph Norman, AMSMI-RD-DP-TT, was the Project Monitor. Dr. James L. Rand was the Program Manager for Winzen and Dr. James S. Wilbeck acted as Principal Investigator. Ms. Pamela G. Scott was responsible for the thermal modeling, Mr. Thomas M. Lew was responsible for the balloon design effort and testing, and Mr. Richard H. Brezinsky was reponsible for material selection and model balloon fabrication.

TABLE OF CONTENTS

LIST OF ILLUSTRATIONS

LIST OF TABLES

1.0 INTRODUCTION

1.1 DISCUSSION

The use of free floating balloons to relay signals over great distances was visualized almost a century ago as evidenced by Patent No. 465,971 granted to Thomas A. Edison in 1891. Since then, both electronics and systems technology have been developed which would permit the establishment of a worldwide communications and surveillance network using free floating balloons in the stratosphere. The availability of such a system is extremely desirable, particularly for military applications. When compared to an orbiting satellite network which is vulnerable during any trans-attack scenario, the free floating long duration balloon network represents an extremely economical, rapidly deployable, and relatively transparent system.

The work horse for the envisioned communication system is the superpressure balloon. Unique characteristics of the superpressure balloon are that it maintains constant volume and that it does not vent lift gas. Maintaining constant volume allows the superpressure balloon to maintain a nominally constant altitude without the use of ballast. Combined with the fact that gas is not vented, this characteristic gives the superpressure balloon the potential for very long duration flight.

1.2 PRACTICAL CONSIDERATIONS

There are, however, various difficulties associated with superpressure balloons which must be addressed. The considerations fall into three main groups: stress considerations, temperature considerations, and material considerations.

The minimization of stress is important for all balloons, but particularly for superpressure balloons. This is because the balloon must not only withstand stresses due to the payload but also those produced by pressurization. It is especially important to avoid local stress concentrations caused by the introduction of forces from the payload into the balloon wall.

Perhaps more important is the prediction and minimization of temperature variations of the lift gas. The temperature differential between the gas and the ambient air (supertemperature) is the driving force behind the level of superpressure of the balloon. The lowest supertemperature expected determines the amount of free lift in the balloon necessary to maintain a positive superpressure at night. The highest supertemperature expected determines the maximum superpressure the balloon must withstand. An accurate forecast of temperature extremes is necessary to prevent either overpressurization or loss in volume.

The third set of considerations concern the balloon material. Most importantly, the material should have a high strength to weight ratio. As mentioned above, the material should help to minimize temperature variations of the lift gas. Another requirement is that the balloon material not allow the escape of gas, whether because of gas permeability or pinhole defects. Also, the material must resist degradation due to the presence of strong ultraviolet radiation in the stratosphere.

1.3 PHASE I TECHNICAL OBJECTIVES AND OVERVIEW

The overall objective of this Phase I effort has been to demonstrate the technical feasibility of producing a reliable constant volume balloon platform which is capable of supporting 50 pounds at 120,000 feet for one year. The approach taken in achieving this objective is outlined below.

(1) A review of superpressure balloon technology was conducted. The review identified previously used balloon shapes and materials, as well as describing past experience with superpressure balloon performance.

(2) Two analytical models were developed to aid in the development of a new superpressure balloon design. A mechanical model served to compare the most promising balloon shapes, estimate stresses, and determine the final balloon design. A thermal model served to compare candidate balloon materials and to predict the superpressure extremes for various flight scenarios.

(3) Research was conducted to find the optimum balloon material. The selection criteria for the material included both mechanical and thermal properties. Once the material was selected, the thermal and mechanical analyses were completed and a final design was developed.

(4) Model balloons were designed and fabricated. Experiments were run to test the performance of the designs. The tests included inflation and burst tests at room temperature and various low temperatures. The results from the tests and the analyses were tabulated and the final report was written.

This report describes, in detail, each of the Phase I tasks. The final Phase I balloon designs are presented in Section 5.3. The report ends with conclusions and recommendations for Phase II.

2.0 STATE OF THE ART IN SUPERPRESSURE BALLOON TECHNOLOGY

An extensive, ongoing review of superpressure balloon technology was conducted to identify approaches to past balloon designs, including any problems identified. In this section, a general review of design shapes and balloon materials is presented. Specific examples of balloon successes and failures are then noted.

2.1 PRIOR DESIGN APPROACHES

2.1.1 Shapes

A number of balloon shapes have been considered for long duration, superpressure applications. Good reviews have been presented by Grass [2-1] and Lally [2-2]. All of the designs which were identified can be placed into one of four categories. These include the cylinder, tetrahedron, sphere, and pumpkin shapes. Each will be discussed in some detail at this time.

2.1.1.1 Cylinder

The cylinder shape has been considered because of its ease of manufacture. Since many thin films are extruded in tubular form, a near cylinder balloon can be fabricated by simply cutting a length of tube and sealing both ends. A larger tube can also be formed by sealing a number of rectangular sheets together. If a flat seal is made, the cylinder takes on the look of a pillow. If the ends are gathered around a small end fitting, they take on a more hemispherical shape. The disadvantage of this design is its large surface area (hence, weight) relative to enclosed gas volume. In practice, this design is rarely used because of its weight inefficiency.

2.1.1.2 Tetrahedron

The tetrahedron, or tetroon, is a simple deviation from the cylinder design. One end is sealed to form a flat pillow seal as mentioned above. At the other end, the pillow seal is rotated 90°, so that the two seals are orthogonal. As with the cylinder, the main advantage of this design is simplicity of manufacture. It also has a greater volume to surface area ratio than the cylinder shape and has been found easier to launch than a cylinder balloon of similar size. Disadvantages include weight inefficiency and stress concentrations at the corners. It is most often used for applications requiring small and inexpensive balloons, such as sounding balloons and balloons used to follow air currents at altitude.

2.1.1.3 Sphere

In theory, the sphere is often considered the optimum shape because it possesses the greatest volume to surface area ratio. Film stresses due to superpressure are relatively low, and there are no points of stress concentration for the perfect spherical shape. The film stress, σ, is given by the relationship:

$$\sigma = \frac{PR}{2t} \qquad (2-1)$$

where P is the pressure differential across the balloon wall, R is the sphere's radius, and t is the film thickness. The stresses are biaxial in nature. In practice, a sphere is fabricated from a number of gores cut from flat sheets or panels. The shape becomes more nearly spherical with increased number of gores, with at least 16 to 24 normally employed.

2.1.1.4 Pumpkin

This design, based largely upon zero-pressure balloon designs, uses exaggerated lobing between load tapes to minimize circumferential stresses. Since circumferential stress is related to the effective circumferential radius of curvature, the stresses are lower because of the reduced effective radii of the lobing design. Such a design allows the use of materials which have greater strength in the meridional direction than circumferential. The meridional load tapes reinforce the balloon in the meridional directions.

2.1.2 Materials

For a superpressure balloon, the film material must have high strength and a high modulus to withstand the large stresses due to the superpressure without substantial deformation or balloon failure. A number of monolithic films as well as a number of film combinations, have been considered previously. These are discussed in the following paragraphs.

2.1.2.1 Polyester

Early balloons were fabricated almost exclusively from polyester films, such as Mylar® which is manufactured by Dupont. It was preferred because it displays good strength and toughness over the temperature range of interest, including temperatures down to -70°C. Although it is not directly heat sealable, it can be sealed with pretreated tape with heat activated adhesive. One of the main problems with this type of film is that it is susceptible to pinholing, crease damage, and abrasion.

A film formed by laminating two thin sheets of Mylar® was found to have fewer flaws and increased resilience, with less tendency to develop tiny flaws after the inspection process [2-1]. Bilaminated Mylar® continues today to be the most used film for superpressure balloons.

2.1.2.2 Nylon

Nylon has often been considered for superpressure applications because of its resistance to pinholing and creasing problems. It also has good strength and modulus, though both values have been below that of Mylar®. In the early 1980's, Winzen fabricated balloons from Nylon 6 and Nylon 12 [2-3]. Both versions suffered from the lack of cold temperature ductility with the cold brittleness point of -60°C for Nylon 12 and a somewhat warmer value for Nylon 6. Recent developments in the evolution of biaxially oriented Nylon 6 have greatly increased the strength of this material and show promise for future applications.

2.1.2.3 Composite Films

A number of balloon skins have been developed which consist of a layering of several different films. This combining of two or more films is done to utilize one or more advantages of each film. One type of composite film combines a Mylar® film for strength with a polyethylene film for heat sealing and covering of the pin holes. Typical of this group is Triplex, which has been utilized by CNES [2-4]. A second type of composite film combines a strength member with a vapor-deposited metal layer which is used to reflect most of the incident sunlight. For the PAGEOS program [2-5], a 0.5 mil Mylar® layer was coated with a 2000 Angstrom layer of aluminum on the outside to reflect the sunlight, thereby protecting the Mylar® from the degrading effects of ultraviolet radiation. The aluminum layer also serves to greatly decrease the rate of diffusion of the lifting gas.

2.2 PRIOR EXPERIENCE WITH SUPERPRESSURE BALLOON PERFORMANCE

Since the late 1950's, a large number of flight programs have been conducted using relatively small spherical superpressure balloons. From these programs, we have gained valuable insights into the requirements of a long duration superpressure balloon system. On a number of different occasions, researchers have attempted to scale up these smaller balloons to the 60-100 foot diameter required for the larger payloads, higher altitudes, and longer durations of interest. However, all such attempts have failed.

Grass [2-1] discussed the flight of two 1.5 mil Mylar® spherical balloons which flew in 1961-62. Both balloons had a diameter of 34 feet, a payload of 38 pounds, and flew at an altitude of 70,000 feet. The balloons flew successfully for 9 and 10 days, respectively, before being terminated by a pre-set timer.

Between 1966 and 1968, 146 superpressure sounding balloon flights were conducted under the GHOST (Global Horizontal Sounding Technique) flight program [2-2 and 2-6]. Balloons were designed to carry very small payloads (150 to 350 grams) to altitudes from 1 to 30 km. The formation of frost and ice was a major problem for balloons flying at altitudes of 12 km and below. Many of the balloons flown at altitudes of 16 and 24 km were very successful, flying in excess of 100 days. These balloons were constructed from 1.0, 1.5, and 2.0 mil bilaminated Mylar®, having diameters of only 2 to 4 meters. One interesting comment on balloons flying at 16 km was that "in order to achieve average life in excess of one year at this altitude, a laminate must be used which is less susceptible to pinhole formation than 1.5 mil bilaminated Mylar®." It was also noted that many of the balloons may have been damaged during ascent due to rapid ascent rates (up to 9 m/s) or cold tropopause temperatures (-80°C). Finally, 2 mil polyethylene balloons with a 20 m diameter were unsuccessful at sustained floats at 30 km.

Lastly, Shipley reviewed a number of flight programs conducted by the National Scientific Balloon Facility (NSBF) during the 1970's [2-7]. In 1973, during Project Boomerang, 68 kg payloads were flown at 24 km altitude using 19.5 m diameter spheres. One of the balloons flew for 210 days. Later 204 kg payloads were flown at 29 km altitudes using 39 m diameter spheres of bilaminated Mylar®. Attempts to fly a 55 m diameter Mylar® balloon failed as it was going into float.

2.3 REFERENCES

2-1 Grass, L.A., "Superpressure Balloon for Constant Level Flight," AFCRL-62-824, August 1962.

2-2 Lally, V.E., "Superpressure Balloons for Horizontal Soundings of the Atmosphere", NCAR-TN-28, June 1967.

2-3 Nelson, J.R. and Borgersen, S.E., "Balloon Materials and Designs," Advances in Space Research, Volume 3, No. 6, 1983, pp. 33-43.

2-4 Rougeron, M., "Up to Date CNES Balloon Studies," Proceedings, Tenth AFGL Scientific Balloon Symposium, AFGL-TR-79-0053, 21-23 August 1978, pp. 39-55.

2-5 Stenlund, S.J. and McLellan, B.D., "PAGEOS Fabrication Accuracy and Reliability", Proceedings, Fourth AFCRL Scientific Balloon Symposium, AFCRL-67-0075, September 1966, pp. 133-142.

2-6 Lally, V.E., Carlson, N., Frykman, R.W., Lichfield, E.W., Rickel, A.B., and Verstraete, M., "Superpressure Balloon flights from Christchurch, New Zealand, August 1967 to June 1968," NCAR-TN-38, February 1969.

2-7 Shipley, A., "Advances in Long Duration High Altitude Flights," Advances in Space Research, Volume 1, 1981, pp. 193-206.

3.0 MODEL DEVELOPMENT

3.1 INTRODUCTION

Analytical modeling played a major role in this Phase I project. Two models were developed over the course of the project. One was a thermal model of the superpressure balloon which was used to predict the maximum and minimum supertemperatures of the lift gas. The thermal model was also used in the material selection task. By allowing a comparison of the thermal effects of different balloon materials, the model helped to optimize the choice of balloon material.

The second model developed in this program was a mechanical model. This model was used to determine the maximum pressure differentials across the film and, based upon a design stress, calculate the size of the balloon. The model was also used to perform trade-off studies that optimized the volume to weight ratio of the balloons evaluated.

3.2 THERMAL MODEL

The prediction of supertemperatures is critical to the balloon design for two reasons. First of all, the maximum supertemperature determines maximum expected superpressure in the balloon material (wall). This determines the maximum stress levels for which the balloon must be designed. Secondly, the minimum supertemperature determines the amount of gas in the balloon necessary to prevent loss of volume because of loss of pressure.

In order to predict the maximum and minimum supertemperatures of the balloon gas, an accurate estimate of the high and low steady state temperatures of the balloon gas was needed. This estimate was obtained by solving the equilibrium heat transfer equations of the balloon gas and wall. The solution was done numerically using a modified version of the computer code THERMNEW developed by Carlson [3-1]. The following sections describe the theoretical basis of the thermal model, major assumptions in the model, and the use of the solution code.

3.2.1 Theoretical Background

The heat transfer models for the balloon are taken from work done by Carlson [3-1] and Kreith and Kreider [3-2]. The equilibrium heat balance equations, which implicitly assume a spherical balloon shape, are shown below. (Refer to Appendix A for definition of symbols used.)

Wall

$$\frac{1}{4}G\alpha_{weff}+\frac{1}{2}Gr_s\alpha_{weff}+\epsilon_{gw}\sigma(T_g^4-T_w^4)+CH_{gw}(T_g-T_w)+CH_{wa}(T_a-T_w)-\epsilon_{weff}\sigma(T_w^4-T_{SS}^4)=0 \quad (3-1)$$

Gas

$$G\alpha_{geff}+Gr_s\alpha_{geff}-\epsilon_{gw}\sigma(T_g^4-T_w^4)-CH_{gw}(T_g-T_w)-\epsilon_{geff}\sigma(T_g^4-T_{SS}^4)=0 \quad (3-2)$$

where:

$$\epsilon_{gw}=\frac{\epsilon_g\epsilon_{wir}}{1-r_{wir}(1-\epsilon_g)} \quad (3-3)$$

$$\epsilon_{geff}=\frac{\epsilon_g\tau_{wir}}{1-r_{wir}(1-\epsilon_g)} \quad (3-4)$$

$$\epsilon_{weff}=\epsilon_{wir}\left\{1+\frac{\tau_{wir}(1-\epsilon_g)}{1-r_{wir}(1-\epsilon_g)}\right\} \quad (3-5)$$

$$\alpha_{geff}=\frac{\alpha_g\tau_{wsol}}{1-r_{wsol}(1-\alpha_g)} \quad (3-6)$$

$$\alpha_{weff}=\alpha_w\left\{1+\frac{\tau_{wsol}(1-\alpha_g)}{1-r_{wsol}(1-\alpha_g)}\right\} \quad (3-7)$$

The equations for effective radiative properties are derived from consideration of the multiple pass phenomenon which is characteristic of transparent materials. The equations are apparently extensions of Stoke's equations for total reflectance and transmittance of a transparent material [3-3].

3.2.2 Assumptions

The thermal model developed in Phase I contains several assumptions. Most of them agree with Carlson's assumptions; those that do not are noted. The assumptions are described below.

The first set of assumptions concern the shape of the balloon. There are three parts of the analysis affected by balloon shape: the convection model, the earth/sky radiation model, and the solar radiation models. For the convection model, the balloon was assumed to be a sphere. This assumption simplified analysis because of the relatively plentiful amount of data existing for spheres, as opposed to

most other shapes. Because convection was found not to be a major driving force in the analysis, no attempts to develop models for a more realistic shape were made. Empirical equations for internal and external convection of a sphere were taken directly from Reference 3-1.

Also affected by shape is the earth and sky radiation on the balloon. This radiation is represented by the blackball temperature, which is the temperature that a black ball would have as a result of (only) radiant thermal exchange between it and the earth and sky. Since the available blackball temperature measurements were made using a roughly spherical "black ball", these measurements are only strictly valid for spherical bodies. In order to use blackball data in Phase I, the balloon was assumed to be spherical in this case as well.

Third, the direct and reflected solar radiation on the balloon are affected by shape. The relationship is described as follows. Since the rays of direct solar radiation are parallel, the direct radiation impinging on the balloon is determined by the projection of the surface area normal to the sun's rays. On the other hand, reflected solar radiation reflected back from earth, is not parallel, but diffuse. Therefore, the reflected radiation impinging on the balloon is determined by the total surface area of the balloon facing the earth [3-2]. Until the actual shape was determined, the assumption of spherical shape was again used. This simplifies matters quite a bit. For a spherical balloon, the projection of the surface area toward the sun is equal to one fourth of the total surface area, independent of the angle of the projection. The earthward surface area is simply half the total surface area.

Once the actual shape was determined, the assumption of a spherical shape in calculating solar radiation was no longer used. The effect of the sun's position relative to the balloon then had to be considered. For a vertically elongated balloon, the projected surface area is largest for a sideways projection and smallest for an overhead projection. This suggests that the "hottest" condition might occur at sunrise, when the sun's rays are normal to the vertical. This could not be automatically assumed, however. At sunrise, the sun's rays must travel through more atmosphere than at noon and, thus, are attenuated more. It was initially thought that atmospheric attenuation could make the "hottest" case occur sometime between sunrise and noon. As it turns out, the vertical attenuation of the solar flux at 120,000 feet is only about 0.2 percent. Even if the horizontal attenuation were several times that of the vertical attenuation, the difference in the solar flux reaching the balloon would still be negligible compared to other effects. (For instance, the solar flux varies ±3 percent from average due to the eccentricity of earth's orbit around the sun [3-4]). It was concluded that, for a vertically elongated balloon, the sideways projection should be used in calculating the "hottest" case. The heat balance equations were changed accordingly.

The second set of assumptions concern the equilibrium state of the balloon. First, the model assumes that the balloon is at steady float; therefore, the convection on both the inside and outside of the balloon can be modelled as natural convection. This assumption also allows the effects of adiabatic expansion and contraction to be neglected. Second, the model assumes that the balloon comes to thermal equilibrium relatively quickly compared to the diurnal cycle so that transient heat

Once the appropriate atmosphere is chosen, the actual float altitude is determined. Actual float altitude differs from the nominal float altitude because a superpressure balloon floats at a constant density profile. Since air density changes with temperature and pressure, the float altitude will fluctuate from the nominal float altitude. The balloon was designed to float at an air density of 0.006438 kg/m^3, which corresponds to an altitude of 120,000 feet for an atmosphere identical to the 1962 U.S. Standard Atmosphere [3-7]. The ambient temperature and pressure, therefore, are those which correspond to the design air density.

A typical input file is shown in Table 3-1 below. The balloon in this example is made of 2 mil polyethylene film. The atmospheric conditions correspond to the U.S. Standard Atmosphere; therefore the float altitude is 120,000 feet (36,500 meters) and the ambient temperature is 285°K. No data could be found regarding day to night ambient temperature and density variations, so the altitude, temperature, and pressure are assumed to be constant for both day and night. Albedo and blackball temperature correspond to total cloud cover.

Table 3-1. Example Input File for Thermal Analysis Code

36500.	Daytime Float Altitude, m
285.	Daytime Ambient Temperature, deg K
36500.	Nighttime Float Altitude, m
285.	Nighttime Ambient Temperature, deg K
0.57	Albedo, 0.18 for Clear, 0.57 for Cloudy
194.4	Blackball Temperature, Clear - 214.4 K, Cloudy - 194.4 K
0.0	Delta p Between Gas and Air, Night, mb
22.675	Mass of Payload Plus Balloon Mass, kg
28.9644	Molecular Weight of Air, kg/kmol
4.0026	Molecular Weight of Gas, kg/kmol
0.0028	Solar Absorptivity of Gas
0.00031	IR Emissivity of Lifting Gas
0.001	Solar Absorptivity of Film
0.885	Solar Transmissivity of Film
0.114	Solar Reflectivity of Film
0.031	IR Emissivity of Film
0.127	IR Reflectivity of Film
0.842	IR Transmissivity of Film
4.647	Ambient Daytime Pressure, mb
4.647	Ambient Nighttime Pressure, mb

The output from each computer run gives the equilibrium wall and gas temperatures for day and night. The supertemperatures for the particular case are found by subtracting the ambient air temperature from the gas temperatures. Because of solar radiation, the maximum supertemperature

will occur in the daytime, and the minimum will occur at night (and will probably be negative). To predict the maximum and minimum supertemperatures for a particular flight scenario, cases must be run for all possible atmospheres associated with that scenario, each with and without cloud cover. The maximum and minimum supertemperatures are the highest and lowest out of the whole group. The supertemperature results for various flight scenarios are shown in Section 5.2.

3.3 MECHANICAL MODEL

This section describes the mechanical model developed in this program. Definitions of the symbols used in the analysis are given in Appendix A. The following assumptions were made in this model.

(1) The balloon does not change volume

(2) Film Stress = $(\Delta P R / 2t)$

Assuming that the volume of a superpressure balloon remains constant, it will float at a constant density altitude. Using this assumption, an air density of 0.006438 kg/m^3 was chosen as the float condition. This density corresponds to the air density at a geopotential altitude of 120,000 feet, which was interpolated from Reference 3-7.

The ambient nighttime air pressure was determined using the ideal gas law and the nighttime air temperature from the thermal model. The air temperature corresponded to the largest negative supertemperature condition:

$$P_{a,n} = \rho_a R_u T_{a,n} / M_a \qquad (3-8)$$

A minimum superpressure was specified to ensure that at the coldest temperatures, there would be enough superpressure left in the balloon for it to maintain its shape and, therefore, not change its volume significantly.

The minimum superpressure was added to the ambient nighttime air pressure to get the minimum absolute pressure of the gas inside the balloon:

$$P_{g,n} = P_{a,n} + P_o \qquad (3-9)$$

Since the volume of the balloon is assumed constant and the mass of the gas inside the balloon should not change, its density is also a constant which can be determined from the ideal gas law:

$$\rho_g = P_{g,a} M_g / R_u T_{g,a} \tag{3-10}$$

To determine the worst case pressure condition, the largest positive supertemperature condition was taken from the thermal model. Since the densities of the surrounding air and the lifting gas are assumed to be constant, their respective pressures can be calculated from the ideal gas law:

$$P_{g,d} = \rho_g R_u T_{g,d} / M_g \tag{3-11}$$

$$P_{a,d} = \rho_a R_u T_{a,d} / M_a \tag{3-12}$$

The largest pressure differential across the balloon wall is, therefore:

$$\Delta P_{design} = P_{g,d} - P_{a,d} \tag{3-13}$$

or, combining Equations (3-8) through (3-12):

$$\Delta P_{design} = \tag{3-14}$$

$$\frac{\rho_a R_u}{M_a}\left[\frac{T_{g,d}}{T_{g,a}} T_{a,a} - T_{a,d} + \frac{M_a P_o}{\rho_a R_u}\frac{T_{g,d}}{T_{g,a}}\right]$$

which is shown in Appendix B.

The total buoyant lift under these conditions is:

$$B = W_a - W_g \tag{3-15}$$

$$= g\rho_a V - g\rho_g V$$

$$= gV(\rho_a - \rho_g)$$

The volume of a single sphere is:

$$V_1 = 4/3\pi R^3 \tag{3-16}$$

For the Multiple Intersecting Spheres (MIS) balloon, which is described in Section 5.1, the volume is:

$$V_n = 4/3\pi R^3 + 2(N-1)(\pi R^2 a - 1/3\pi a^3) \qquad (3-17)$$

which is derived in Appendix C.

The buoyancy must be balanced by the payload and the balloon weight. The following components make up the total balloon weight:

(1) Film Weight
(2) Belt Weight
(3) Tape Weight
(4) Load Line Weight

The model currently does not take into consideration the end fitting weights, nor the weights of the loops that will hold the load lines in place. Since virtually all variables depend upon the balloon radius and, for the MIS balloon, the separation distance, the equations derived use these values as input. The remaining variables can be readily calculated and iterated to the desired payload.

Film weight is determined by the balloon's surface area and film thickness. The surface area of a single sphere is:

$$SA_1 = 4\pi R^2 \qquad (3-18)$$

The surface area for MIS is derived in Appendix C, and is given by the formula:

$$SA_n = 4\pi R^2 + (N-1)4\pi R a \qquad (3-19)$$

The required balloon wall thickness is calculated by:

$$t = \frac{\Delta P R}{2\sigma} \qquad (3-20)$$

Total film weight is then:

$$FW = SA t \rho_{film} \qquad (3-21)$$

The weight of the reinforcing belt will depend upon its required strength. The following derives the required strength of the reinforcing belt. Referring to Figure 3-1, the net outward radial force per unit by length on the belt, caused by the film stress, is determined by:

$$T = 2[\sigma t \cos\theta] \qquad (3-22)$$

$$= \Delta P R \cos\theta$$

By summing the forces in the radial direction, we arrive at the actual tension in the belt. This is shown in Figure 3-2 which is a top view of a section of the reinforcing belt.

$$\sum F_r = 0 = T r_b d\phi - 2H \sin d(\phi/2) \qquad (3-23)$$

For small angles ϕ:

$$2H d\phi/2 = T r_b d\phi \qquad (3-24)$$

and using Equation (3-22),

$$H = \Delta P R \cos\theta r_b \qquad (3-25)$$

It was assumed that the belt for the MIS balloon would consist of a number of Kevlar cords, each with a breaking strength of 500 pounds. A termination fitting for connecting the ends of the belt was not taken into consideration.

The total tape weight was calculated by assuming a maximum gore width for the film and determining the number of taped seals that would be required. Each seal had a one-inch wide tape placed on the inside and the outside of the joint. The tape was of the same thickness as the balloon wall, with a 0.25 mil thick coating of adhesive on one side of the tape. The adhesive had a specific gravity of 1.0.

The load line length is given by:

$$L = \frac{R\pi}{2} + 2(N-1)\alpha + R\gamma + \frac{R}{\tan\gamma} \qquad (3-26)$$

as illustrated by Figure 3-3.

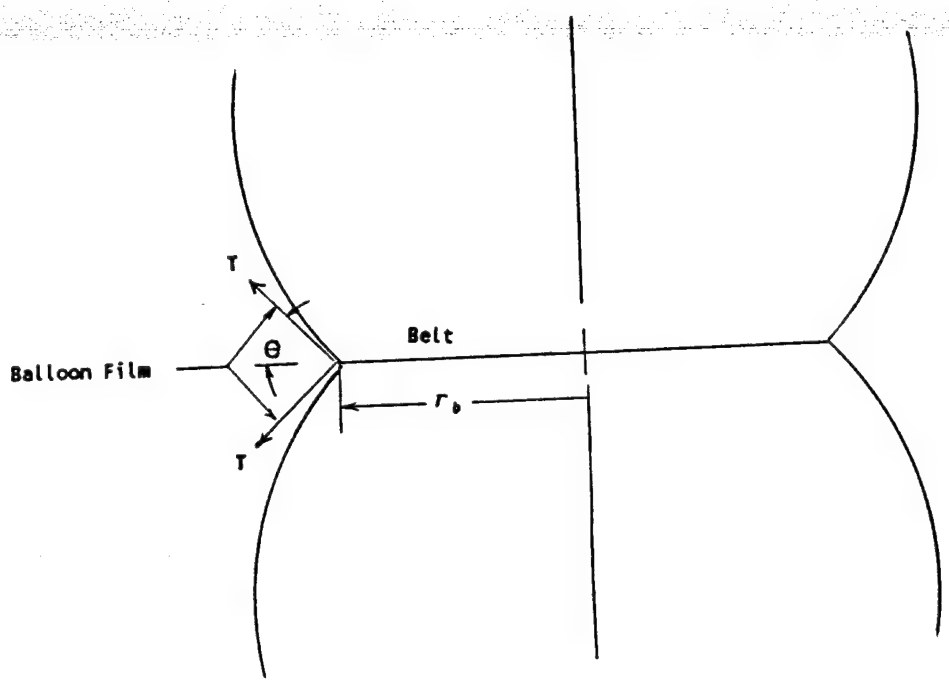

Figure 3-1. Belted Balloon

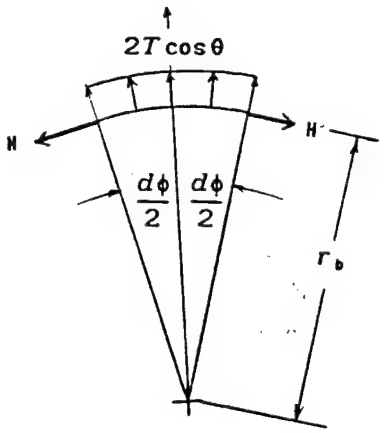

Figure 3-2. Diagram of Forces Acting on Belt

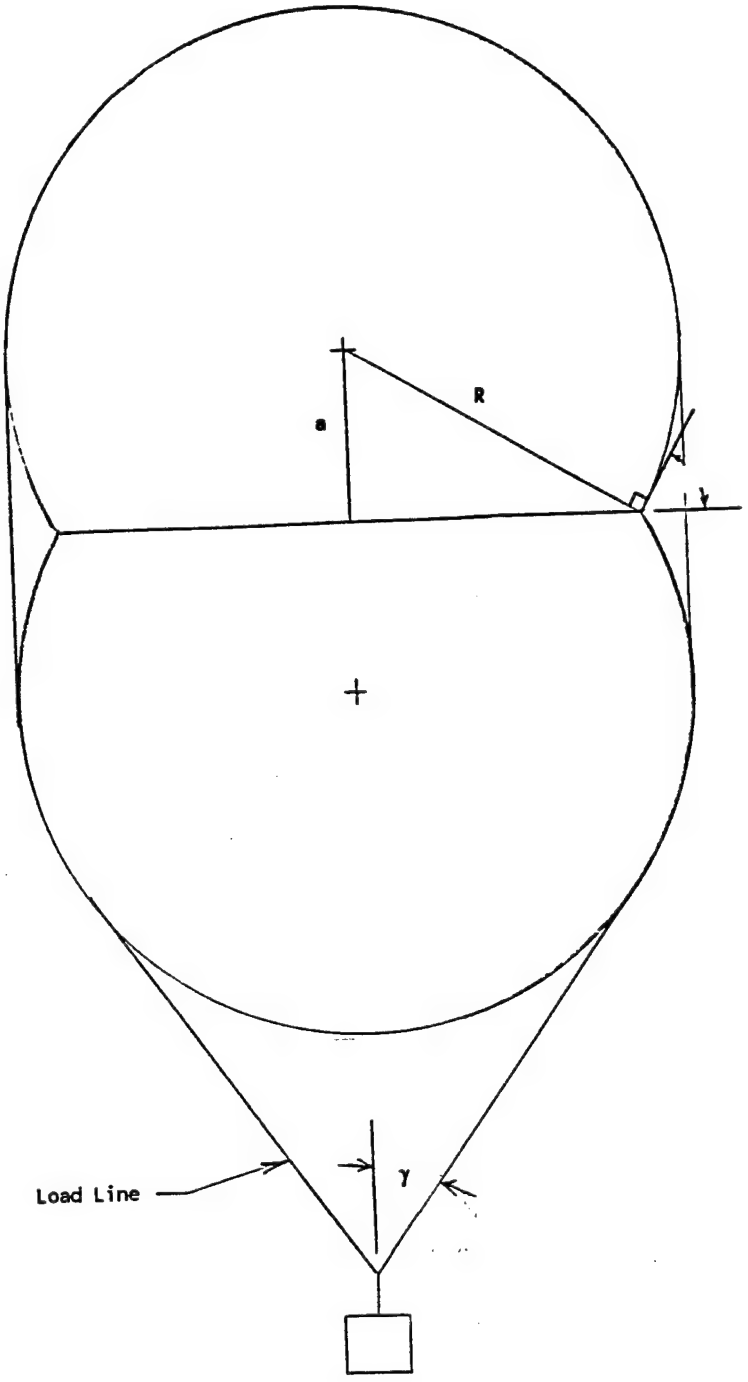

Figure 3-3. Load Line Arrangement

3.4 REFERENCES

3-1 Carlson, L.A., "THERMNEW - A Preliminary Model and Computer Program for Predicting Balloon Temperatures at Float," TAMRF-921C1-79101, October 1979.

3-2 Kreith, F. and Kreider, J.F., "Numerical Prediction of the Performance of High Altitude Balloons," NCAR Technical Note, NCAR-IN/STR-65, February 1974.

3-3 Kreith, F. and Kreider, J.F., Principles of Solar Engineering, McGraw-Hill Book Company, New York, 1978.

3-4 Incropera, F.P. and DeWitt, D.P., Introduction to Heat Transfer, John Wiley and Sons, New York, 1985.

3-5 Lucas, R.M., and Hall, G.H., "The Measurement of Balloon Flight Temperatures Through Sunset and Sunrise," Proceedings, Fifth AFCRL Scientific Balloon Symposium, Ed. Lewis A. Grass, AFCRL-68-0661, December 1968.

3-6 Carlson, L.A. and Horn, W.J., "A Unified Thermal and Vertical Trajectory Model for the Prediction of High Altitude Balloon Performance," Aerospace Engineering Department, Texas A&M University, TAMRF Report No. 4217-81-01, June 1981.

3-7 Warren, J.C., Smalley, J.H., and Morris, A.L., "Aerostatic Lift of Helium and Hydrogen in the Atmosphere," NCAR Technical Notes, December 1971.

4.0 MATERIAL SELECTION

The criteria for selecting a balloon material are divided into two main areas: mechanical properties and thermal properties. The major emphasis of the selection task was to develop a layered material which, as a composite, would optimally satisfy the criteria in both areas. This section will discuss the desired mechanical and thermal properties along with the advantages and disadvantages of several materials considered. The section will be concluded with a description of the final material choice for this Phase I effort.

4.1 MECHANICAL PROPERTIES

The desired mechanical properties of the balloon material were specified at the start of this program. They include the following:

(1) High biaxial tensile strength
(2) High tensile modulus
(3) Toughness in tear and abrasion resistance
(4) Cold temperature ductility
(5) Thin gage
(6) Low permeability to helium and hydrogen
(7) Resistance to pinholing and creasing
(8) Sealability
(9) UV stability

Initially, it was thought unlikely that any single material could satisfy all the above criteria as well as possess good thermal properties. Therefore, the balloon wall was not restricted to any one material. Rather, it was envisioned that a layered film could be developed in which each layer would serve a different function. One layer would be the "strength member," and would provide roughly the first seven mechanical properties. The selection of the strength member layer received the most emphasis in Phase I because of its relative importance. If necessary, another layer would be the "sealing member" to provide good sealability. UV stability could be provided by still another layer. One or more of these layers would also be chosen based upon their thermal properties, as discussed in the next section. The layered concept allowed a much broader range of materials to be considered as candidate wall materials.

A number of film materials were considered for the strength member during the material selection process. A list of commercially available films which appear best suited for balloon applications is given in Table 4-1. As a strength member, polyethylene has many of the desired features, such as high elongation, cold temperature ductibility, thin gage, and resistance to pinholing and creasing. Its

disadvantages are its low modulus, which would result in significant increases in volume during daytime, and its low strength. All of the other films display higher moduli and tensile strengths, with the highest values occurring for the oriented films. Mylar® has been the choice for fabrication of superpressure balloons in the past because of its good strength and very high modulus. However, it exhibits a low resistance to pinholing and creasing, causing the effective strength to be dramatically reduced in design applications at the very cold temperatures. Recently, Emblem® (a biaxially oriented nylon) has been developed with superior strength and good resistance to pinholing and flex cracking.

Table 4-1. Mechanical Properties of Commercially Available Films (Room Temperature)

Film	Density $lb/inch^3$	Modulus $lb/inch^2$	Ultimate Tensile Strength $lb/inch^2$	Elongation %	Ref.
Lexan® (polycarbonate)	0.044	275,000	11,000	100-150	4-1
Mylar® (polyester)					
-MD*	0.049	550,000	24,000	125	4-2
-TD*	0.049	550,000	31,000	95	
Capran® 77 (extruded Nylon 6)					
-MD	0.041	90-110,000	10-16,000	375-500	4-3
-TD	0.041	105-125,000	10-16,000	375-500	
Emblem® (biaxially oriented Nylon 6)	0.042	200-310,000	28-36,000	70-110	4-4
Stratofilm® 372 (linear-low density polyethylene)					
-MD	0.033	15,000	6,800	925	4-5
-TD	0.033	15,000	5,100	1125	
Polypropylene					
-Extruded	0.032	-	4,500-10,000	550-1000	4-6
-Biaxially oriented	0.033	-	7,500-40,000	35-475	4-6

**Note:* *MD - Meridional direction of the film*
TD - Transverse direction of the film

Although the highly oriented films display improved mechanical properties for this application, they do have one major drawback. They will lose their orientation and, hence, their improved prop-

erties if heated above the shrink temperature. Thus, these films cannot be heat sealed directly because of the high temperatures required. For this reason, an adhesive layer was sought for the material chosen.

A number of requirements were chosen for the adhesive layer. If heat activated, it is required that the activation temperature be below the shrink temperature of the film. For the Emblem film, this temperature is on the order of 400°F. It was also required that the resulting seal be as strong as the virgin film both at room and cold temperatures and under long term creep conditions. Finally, it was required that an adhesive be chosen which could be applied and activated in an automated sealing system with minimal problems.

Before surveying the available adhesives, a decision had to be made as to the geometry of the seal. With polyethylene balloons, the film is heat sealed to itself in a peel seal configuration. This is allowed since the film is actually melted and the resulting bond is strong in tension. However, adhesive bonds are normally much stronger in shear than in tension. Adhesively bonded peel seals are especially susceptible to creep loads. Thus, the decision was made to utilize either lap seals or butt seals. In a lap seal, a layer of material overlaps another layer with adhesive between the two. In a butt seal, the two layers are butted against each other and a tape layer is laid over the joint. After much consideration, the butt seal was chosen since the adhesive can be applied directly to the tape. The adhesive would only come in contact with the film at the time of sealing. This should greatly simplify the fabrication process.

Room temperature curable, pressure sensitive, and hot melt adhesives were all considered. The curable adhesives have the potential for chemical reaction with the nylon surface; therefore, they offer potentially the strongest bonds. However, they have several drawbacks. Their shelf life is so short that they would need to be made and used on the same day. Secondly, if a tape is applied incorrectly, the tape can be lifted off the surface and reapplied, but some of the adhesive would be left on the film. This residue would have to be cleaned to prevent unwanted bonds at some later time. The tape would also have less adhesive than that considered optimum. Also, a technique would have to be developed for applying the adhesive to the tape during the actual automated sealing process since prior application would result in a chemical reaction with the tape prior to sealing. Finally, the low initial bond strength would require that the sealed areas not be stressed until the adhesive has cured sufficiently to form a strong bond.

A pressure sensitive adhesive system has fewer disadvantages. The tape can be manufactured well in advance of its use. By applying the adhesive directly to the tape and then applying a release film (that is, a film with very poor adhesion to the adhesive) to the other side of the adhesive, the tape can be wound on a roll for storage and ease of use. The release strip is simply peeled off the tape prior to its application to the seal. The full strength of the bond would be obtained initially so that the

seal can easily bond the stresses generated during the manufacturing process. However, a misapplied tape would be very difficult to correct for this same reason. During an automated seal process, this would place great constraints on the system for proper alignment and tape application.

A hot melt adhesive would share the same advantages of the pressure sensitive tape without the extreme stickiness. During sealing, the adhesive tape could be aligned with edges to be sealed prior to the application of sufficient heat and pressure to cause a good seal. Also, since the adhesive would not be activated at room temperature, the film could be stored on a roll without the need of a release strip. A constraint on the adhesive would be that activation must occur at a temperature well below the shrink temperature of the nylon.

With regard to UV resistance, several options were considered. One option is to deposit a very thin metallic layer on the outside of the strength member. An advantage to this option is that it would also provide an excellent gas barrier. Another option is to use an additive to the strength member, such as an antioxidant or a UV absorber.

4.2 THERMAL PROPERTIES

The thermal properties relevant to the "thermal member" of the balloon wall are the radiative properties. These include absorptivity, α, emissivity, ϵ, reflectivity, ρ, and transmissivity, τ. These properties are not independent but follow the relationships given below:

$$\alpha_\lambda + \rho_\lambda + \tau_\lambda = 1 \qquad (4-1)$$

$$\alpha_\lambda = \epsilon_\lambda \qquad (4-2)$$

where λ is the wavelength of interest. For many engineering applications, the radiative properties can be spectrally averaged to take away the dependence on wavelength. Unfortunately, this is not true for balloon heat transfer. This is because the heat transfer is occurring over two different parts of the electromagnetic spectrum, the solar and the infrared (IR). Since there is very little overlap in the solar and IR spectrum, the radiative properties averaged over each spectrum can be widely different. An example of this is snow, which is highly reflective to solar radiation (α_{solar} is small) but highly absorptive to IR radiation. Therefore, radiative properties of the thermal member must be known for both the solar and IR spectrums.

Early on in the program, it was noted that the desired combination of thermal member radiative properties are low solar absorptivity and high IR emissivity. Lower solar absorptivity means that the balloon will absorb less of the sun's energy during the day. Higher IR emissivity means that the balloon is a more efficient emitter of heat. One might question this logic by noting that, according to Equation (4-2), this automatically specifies that the balloon will be highly absorptive of IR and a poor emitter in the

solar spectrum. As it turns out, the contribution of IR radiation to the maximum supertemperatures of the balloon is negligible. Furthermore, a poor emissivity in the solar spectrum is inconsequential, since the balloon's temperature is too low for the balloon to emit in that spectrum.

Another desirable radiative property of the thermal member is opacity to solar radiation ($\tau_{solar} = 0$). This would prevent the lift gas from being heated directly from the sun. Complete opacity would be even better so that the radiative properties of the substrate layers would have no adverse effects on thermal performance. Also, an opaque surface would decouple the thermal analysis from its dependency on the very uncertain gas radiative properties.

A review of the radiative properties of various substances provided a starting point for determining candidate thermal layers [4-7 through 4-11]. These include data from several reports of space shuttle experiments which tested thermal control coatings for use in the space environment. Table 4-2 shows absorptivity and emissivity for several materials which had low $\alpha_{solar}/\epsilon_{IR}$ ratios, along with black paint, gold, and aluminum foil for comparison.

To compare different materials on the basis of balloon performance, the thermal model described in Section 3.0 was used. Calculations for each material were based on the same hypothetical atmosphere in which the daytime temperature corresponds to the first percentile high temperature recorded for 120,000 feet and the nighttime temperature corresponds to the first percentile low temperature for that altitude. They were all done for both cloudy and clear conditions, and the most extreme result were used. The calculations confirmed that the smallest diurnal temperature variations were usually achieved for materials with the lowest $\alpha_{solar}/\epsilon_{IR}$ ratios. The results from a set of comparisons are shown in Table 4-3.

The first case analyzed was polyethylene. Since Winzen produces this film and has radiative property data for it on hand, this case was used as a point of comparison. Judging from the extremely low $\alpha_{solar}/\epsilon_{IR}$ ratio of polyethylene, this material should have given the smallest temperature variation. It did not because of its very high transmissivity in the solar spectrum. The transmissivity allowed the solar radiation to pass through the film and heat the gas directly. This is a good example of why transmissivity of the thermal layer is undesirable.

The second case analyzed was aluminized Mylar®, with the aluminum side facing outward. (Note that since aluminum is opaque to radiation, the radiative properties of the Mylar® side do not come into play. The case of an aluminum thermal member would have identical results.) Before the importance of a low $\alpha_{solar}/\epsilon_{IR}$ ratio was recognized, the idea of using aluminized Mylar® was appealing. The aluminum creates a good gas barrier and placed on the outside, gives the Mylar® strength member protection from UV radiation. As shown in the results, however, this case is completely unacceptable. Although the absorptivity is low, the emissivity is simply not high enough to keep the balloon relatively cool.

Table 4-2. Solar Radiative Properties for Various Materials				
Material	α_{solar}	ϵ_{IR}	$\alpha_{solar}/\epsilon_{IR}$	Reference
Aluminum				
Anodized	0.14	0.84	0.17	4-8
Foil	0.15	0.05	3.00	4-8
Paints				
White, acrylic	0.26	0.9	0.29	4-8
White, Zinc Oxide	0.16	0.93	0.17	4-8
Magnesium Oxide	0.14	0.73	0.19	4-7
ZnO/Potassium Silicate	0.17	0.9	0.19	4-9
ZnO/Silicone	0.19	0.81	0.23	4-9
Methyl Silicone	0.22	0.81	0.27	4-9
PVC Terpolymer (VMCH)	0.23	0.44	0.52	4-9
Capran® 77	0.12	0.906	0.13	4-3
Silvered FEP Teflon (5 mil)	0.11	0.8	0.14	4-10
Silvered FEP Teflon (2 mil)	0.06	0.68	0.09	4-10
Kapton	0.48	0.81	0.59	4-10
Fabric (FEP/Al)	0.2	0.68	0.29	4-10
Fused Silica, Silvered on Back	0.07	0.78	0.09	4-11
Optical Solar Reflector	0.05	0.76	0.07	4-9
Black Paint	0.98	0.98	1.00	4-8
Gold	0.22	0.025	8.80	4-7

Emissivities are given for material temperatures of about 300°K

It was found that the emissivity of reflective metals can be increased dramatically by surface treatment, leaving the absorptivity unchanged. The third case shows the relatively moderate temperature swing resulting from an anodized aluminum surface. Similar results were achieved for an FEP Teflon coated aluminum material. Even better results were achieved with silvered FEP Teflon, the fourth case shown. The improvement is because the silver surface tends to reflect directly, while the aluminum surface tends to reflect diffusely. The more directly reflected radiation is less likely to be absorbed in the Teflon layer before escaping.

The problem with both of the polymer coated metals was thickness. None of the data in the literature were for thicknesses below 2 mil. Since the polymer coated metal could not double as the strength member, the weight penalty of a thermal layer this thick would be too great. A calculation was made to determine how emissivity of the polymer changes with thickness based on theoretical considerations. It was found that thicknesses on the order of one tenth mil would give virtually no enhancement of emissivity of the bare metal. Before an investigation of anodized aluminum could begin, metallic elements of any kind were ruled out because of radar reflectiveness.

The last case shown in Table 4-3 is an extruded nylon 6 film. This case results in a fairly moderate temperature swing. It is interesting to note that, although the $\alpha_{solar}/\epsilon_{IR}$ ratio for Capran® 77 is larger than that for polyethylene, the temperature swing was smaller. This is a consequence of transmissivity effects. Capran® has a much smaller solar transmissivity than polyethylene; therefore, less solar energy was able to heat the gas directly.

Table 4-3. Predicted Temperature Extremes for Superpressure Balloon at 120,000 Feet

Balloon Material	α_{solar}	ϵ_{IR}	$\alpha_{solar}/\epsilon_{IR}$	Nighttime Gas Temperature, °C	Daytime Gas Temperature, °C	Temperature Variation, C°
Single Layer Polyethylene	0.001	0.031	0.03*	-76	-9	67
Aluminized Mylar®, Aluminum Side Out	0.14	0.03	4.7	-75	+110	185
Anodized Aluminum Surface	0.14	0.84	0.17	-78	-34	44
Silvered FEP Teflon (2 mil)	0.06	0.68	0.09	-78	-43	35
Capran® 77 Film	0.12	0.906	0.13*	-78	-19	59

**Since this material is transmissive, the use of $\alpha_{solar}/\epsilon_{IR}$ for predicting thermal performance is not strictly applicable.*

At this point, it is important to note that there is some uncertainty in the results because of the difficulty in obtaining reliable radiative properties. Transmissive materials, like polymers, are especially troublesome. The measurement of absorptivity and emissivity is significantly more complicated for these materials. Relative errors in measurement increase with increasing transmissivity. Also, the unavailability of radiative data for Emblem® make it necessary to use the properties of Capran® 77. Although both materials are nylon 6 films, it is not actually known how closely the radiative properties agree. These problems will be addressed in Phase II.

The placement of the thermal member with respect to other layers of material is critical to the balloon thermal performance. Ideally, the thermal member should interact unobstructed with the radiation impinging on the balloon. If some other layer is on top of the thermal layer, its radiative properties must be considered.

WINZEN INTERNATIONAL, INC.

12001 NETWORK BOULEVARD - SUITE 200
SAN ANTONIO, TEXAS 78249

TELEPHONE: (512) 692-7062

April 14, 1989

Commander
U.S. Army Missile Command
Redstone Arsenal, AL 35898-5244

Attention: AMSMI-RD-DP-TT/Dr. Ralph Norman

Reference: Final Report
Contract No. DAAH01-88-C-0715
WII Project No. 9942-01
"Long Duration Balloon Technology Survey"

Dear Dr. Norman:

Enclosed is a copy of the final report on the reference contract. We are also mailing seven other copies, per the attached distribution list. We enjoyed working on this effort and feel that we were very successful in demonstrating feasibility of a long duration balloon platform.

Respectfully submitted,

James L. Rand
Principal Investigator

JLR/cds

Attachment

4.3 FINAL MATERIAL CHOICE

As was noted in the previous subsection, good properties in one area often detract from the properties in the other area. As a consequence, a considerable amount of iterations occurred between the mechanical and thermal areas of the material selection task. The final choice, therefore, was the result of a compromise between the two.

The biaxially oriented nylon 6 film, Emblem®, was chosen as the strength member because of its high modulus, high tensile strength, and tolerable thermal properties. However, the tear strength is very low which is a characteristic of high modulus films. This property virtually guarantees that the system will fail catastrophically in the presence of a flaw or other damage while pressurized. This property may be mitigated by laminating a thin layer of a compatible material to the Nylon strength member. Unfortunately, a severe weight penalty must be paid to add a thin layer of film with improved "toughness". It was therfore decided to proceed with the Emblem® film until such time as the minimum required tear strength can be quantified.

Despite considerable efforts to find a good thermal coating, none was identified. For all opaque and/or reflective coatings considered, the increased weight of the coating greatly exceeded its benefits. The adhesive chosen for this application was a polyamide hot melt adhesive from the Union Camp Corporation. The adhesive, trade named UNI-REZ 2654, was chosen because of its reported good low temperature impact properties.

4.4 REFERENCES

4-1 "Plastics, 1987 Properties Guide," GE Plastics, General Electric Company, Plastics Group, Pittsfield, Massechusetts, 1987.

4-2 "Mylar® Polyester Film for Packaging: Technical Brochure," El DuPont De Nemours & Company (Inc.), Polymer Products Division, Wilmington, Delaware.

4-3 "Capran® 77C, Polyamide Film: Technical Data," Allied Fibers and Plastics Company, Engineered Plastics Division, Morristown, New Jersey.

4-4 "Emblem®, Biaxially Oriented Nylon Film: Technical Brochure," Unitika, Ltd., Osaka, Japan, 1987.

4-5 "Stratofilm® Specifications," Winzen International, Inc., San Antonio, Texas, 1988.

4-6 Modern Plastics Encyclopedia, Volume 64, Number 10A, McGraw-Hill, Inc., New York, New York, October 1987.

4-7 Kreith, F. and Kreider, J.F., Principles of Solar Engineering, McGraw Book Company, New York, 1978.

4-8 Incropera, F.P. and DeWitt, D.P., Introduction to Heat Transfer, John Wiley and Sons, New York, 1985.

4-9 Millard, John P. and Pearson, B.D., Jr., "Optical Stability of Coatings Exposed to Four Years Space Environment on OSO-III, "AIAA 8th Thermophysics Conference, AIAA Paper No. 73-734, 16-18 July 1973.

4-10 Hall, D.F. and Fote, A.A., "α_s/ϵ_h Measurements of Thermal Control Coatings Over Four Years at Geosynchronous Altitude, " AIAA 18th Thermophysics Conference, AIAA Paper No. 83-1450, Montreal, Canada, 1-3 June 1983.

4-11 Hitchcock, M.F., "A Review of Polymeric Satellite Thermal Control Material Considerations," SAMPE Journal, September/October, 1983.

5.0 DESIGN

Most of the actual design of the superpressure balloon occurred before the material selection was made. Two candidate balloon shapes were designed using an assumed material in order to conduct tradeoff studies between them. Also, a payload attachment method was developed. Once the material had been selected, the design analysis proceeded to completion. The thermal balloon model was used to calculate the expected supertemperatures for specific flight scenarios. The supertemperature extremes were used to calculate the superpressures for use in the mechanical model. A "first cut" balloon was designed on the basis of the calculated superpressures. Since the thermal model is dependent on shape and size, a new set of thermal calculations were performed. This section will first recount the design process, describing the various tradeoffs which contributed to the final design of the balloon. Second, the final results from the thermal analysis will be discussed. Third, the final design based on the expected supertemperatures will be described.

5.1 SUPERTEMPERATURE PREDICTIONS

Once the material selection was made, the thermal model described in Section 3.2 was used to predict the preliminary supertemperatures based on an assumed balloon size and the Standard Atmosphere. At that time, a balloon film had not yet been chosen. It was assumed that the thermal properties of the chosen film would be better than that for polyethylene; therefore, calculations based on polyethylene would be conservative. As shown in Table 4-3, the resulting temperature variation for a polyethylene balloon was 67°C. A balloon was then approximately sized based on this variation. This approximate balloon size was used to make the final supertemperature predictions for various flight scenarios.

The first scenario to be considered corresponds to the probable conditions of the first long duration test flight of the balloon: Sao Paulo, 23°S, in the winter. Since atmospheric data for southern latitudes were not available, it was assumed that atmospheric data for northern latitudes are reasonable approximations for atmospheres at corresponding southern latitudes. The nearest latitudes to 23° for which we had data were 15° and 30°. Therefore, these latitudes were used to make supertemperature predictions for the Sao Paulo flight. It is thought that 15° and 30° represent reasonable latitude extremes for the test flight, considering the small amount of North-South drifting the balloon will experience at this time of year. The predicted temperature extremes for the test flight are shown in Table 5-1.

Of these cases, the maximum supertemperature is +9°C resulting from a clear day at 30° latitude. The minimum supertemperature is -49°C, resulting from a cloudy night at 15° latitude. This is a swing of 58°C in supertemperature.

This swing is over twice as large as the 25° swing used for designing superpressure balloons in the past. The reason for the discrepancy between the earlier estimate and the current one could have arisen from the choice of atmospheric extremes. It is possible that the atmospheric extremes used in this analysis are quite rare, and that more moderate atmospheres should be used in future predictions. It is also possible that the earlier estimate is unrealistically low. Unfortunately, the basis for the earlier estimate is not known. Until the probabilities for various atmospheric extremes are known, the supertemperature variation predicted by the Phase I thermal model will be used.

Table 5-1. Predicted Temperature Extremes for a Flight from Sao Paulo.

Atmosphere	Cloud Conditions	Ambient Temperature, °C	Night Gas Temperature, °C	Day Gas Temperature, °C
15°	Cloudy	-26	-75	-33
15°	Clear	-26	-57	-21
30°, January	Cloudy	-30	-75	-33
30°, January	Clear	-30	-57	-21

**Note: Atmospheric data is from northern latitudes. It is assumed that data from northern latitudes reasonably approximates data for southern latitudes.*

For the sake of completeness, supertemperature calculations were also done for atmospheres which represent the extremes for the globe. As the latitude increases, there is a wider variation of ambient temperature between winter and summer. There are also cold and warm "regimes" documented for the upper latitudes. Table 5-2 shows the predicted temperature extremes for 60°N latitude and polar atmospheres. Note that there is no daytime calculation for the polar winter since there is no sun during this time. The reverse is true for the polar summer case.

Table 5-2. Predicted Temperature Extremes for a Balloon between 60°N and the Pole.					
Atmosphere	Regime	Conditions	Ambient Temperature, °C	Night Gas Temperature, °C	Day Gas Temperature, °C
60°N, January	Cold	Cloudy	-66	-78	-34
60°N, January	Cold	Clear	-66	-59	-22
60°N, January	Warm	Cloudy	-38	-76	-33
60°N, January	Warm	Clear	-38	-58	-21
60°N, July	-	Cloudy	-19	-74	-33
60°N, July	-	Clear	-19	-56	-21
Polar Winter	-	Cloudy	-75	-79	-
Polar Winter	-	Clear	-75	-60	-
Polar Summer	-	Cloudy	+19	-	-31
Polar Summer	-	Clear	+19	-	-20

5.2 BALLOON DESIGN PROCESS

5.2.1 Preliminary Design Considerations

Balloon shape was the first aspect to be considered in the balloon design process. The paragraphs below discuss each of the candidate balloon shapes, giving the advantages and disadvantages of each. The results of a tradeoff study comparing the two are also given.

The first shape to be considered was the sphere. As noted in Section 2.0, the spherical shape has several advantages. First, the spherical balloon is simple to design and fabricate. Also, the stress distribution is relatively constant from top to bottom, and is closely approximated by the simple relationship PR/2t. In the past, the sphere has been chosen because it is an efficient pressure vessel

shape in that it maximizes the volume to surface area ratio. It is important to note, however, that surface area is only one of the determining factors in balloon weight. Material density and thickness are two other factors that affect balloon weight.

The second and much more novel shape to be considered was the Multiple Intersecting Spheres (MIS). The MIS is a shape which was earlier considered by Titan Systems for use in studies of Mars [5-1]. The concept consists of a vertical column of two or more intersecting spheres. The distance between the centers of the intersecting spheres can be between zero and two times the radius for spheres of equal radius. For spheres of different radii, r_1 and r_2 where $(r_1 < r_2)$, the distance between the intersecting spheres' centers can range between $(r_1 - r_2)$ and $(r_2 + r_1)$. The distance between the spheres can be optimized to maximize the volume to weight ratio.

An important factor in the design of the MIS shape is controlling the stress at the intersection of the spheres. Analysis has shown that the intersection area will develop very high circumferential loads. A reinforcing belt will be placed in that region to carry those loads.

The advantage of the MIS shape over the single sphere balloon is a better volume to balloon weight ratio. While the MIS has a poorer volume to surface area ratio when compared to the single sphere, it has a much better volume to balloon weight ratio because the radius of curvature is reduced. A smaller radius of curvature causes lower stresses; therefore, the required thickness of the balloon wall can be reduced.

A problem with both the spherical and MIS shapes is that of payload attachment. For both the sphere and the MIS shapes, payload attachment at the balloon base fitting theoretically causes the meridional stresses to be infinite. This is due to the balloon material at the base being perpendicular to the hanging weight.

Efforts to avoid the high stresses have often been unsuccessful. Several examples of these efforts were found in Reference 5-2. They included patches and lines, tabs and lines, bonded webs, and flat caps. Each of these methods were tested in a cold chamber at Wright-Patterson Air Force Base. In each case, shrinkage of components at -80°C over-stressed the model balloon, causing it to fail. A satisfactory method called the great circle design was eventually developed. Load lines which were looped over the top of the balloon supported the payload. The load lines were not fixed to the balloon wall, but were free to slide through small restraining loops which were evenly spaced along the gore length.

Without knowledge of the great circle design, Winzen developed a similar payload attachment method which was thought to be original. In this method, the payload is hung from Kevlar lines threaded through loops which are sealed to the balloon. The method, which is described fully in

Section 5.3, avoids stress concentrations at payload attachment points. When it was discovered that the great circle design was the preferred choice in Reference 5-2, the decision was made to use this method in the final design.

A tradeoff study was performed to compare the physical characteristics of the single sphere balloon and the MIS. Initially, it was assumed that the MIS balloons should consist of spheres of decreasing radius, with the largest on top. Tapering the radii from top to bottom was considered necessary to prevent the load lines from squeezing the lower spheres. After some thought, it was concluded that the load line pressure on the lower spheres would be no more detrimental than the pressure from the load lines running along the topmost sphere. Since intersecting spheres of different radii were less efficient, it was decided to study only MIS shapes with equal radius spheres.

Several balloons of each type were designed for the tradeoff study, with the radius increasing in five foot increments. For each radius, the required film thickness, the resulting balloon weight, and the total lift were calculated. In the tradeoff study, balloon weight consisted only of film weight. The payload capacity was then computed as the difference between the total lift and the balloon weight. Although the nominal payload for this program is 50 pounds, data points used in the study included balloons with payload capacities of 50 pounds and more. This was done because the miscellaneous weights (seal, fittings, and load line weights) had not yet been determined and these weights increase the effective payload.

The following assumptions were made for the tradeoff study. The lifting gas is helium under a minimum superpressure of 0.166 mbar. The float altitude is 120,000 feet. The film for the balloon wall was Mylar® with a density of 0.00728 pounds/ft^2/mil. The design stress was 10,000 psi. For the study, the MIS consisted of three spheres of equal radius. The distance between the centers of the intersecting spheres was optimized to provide the greatest volume to surface area ratio.

For the same balloon weight, the MIS shape can carry significantly more payload than the single sphere. This is due to the fact that the lower stress in the MIS shape allows a thinner film layer than the single sphere shape. Figure 5-1 is a plot of the balloon weight versus payload capacity. Figure 5-2 is a plot of balloon radius versus payload capacity. The results of the tradeoff study are shown in Table 5-3.

In view of the much better performance of the MIS in the tradeoff study, it is this shape which will be used in the final design.

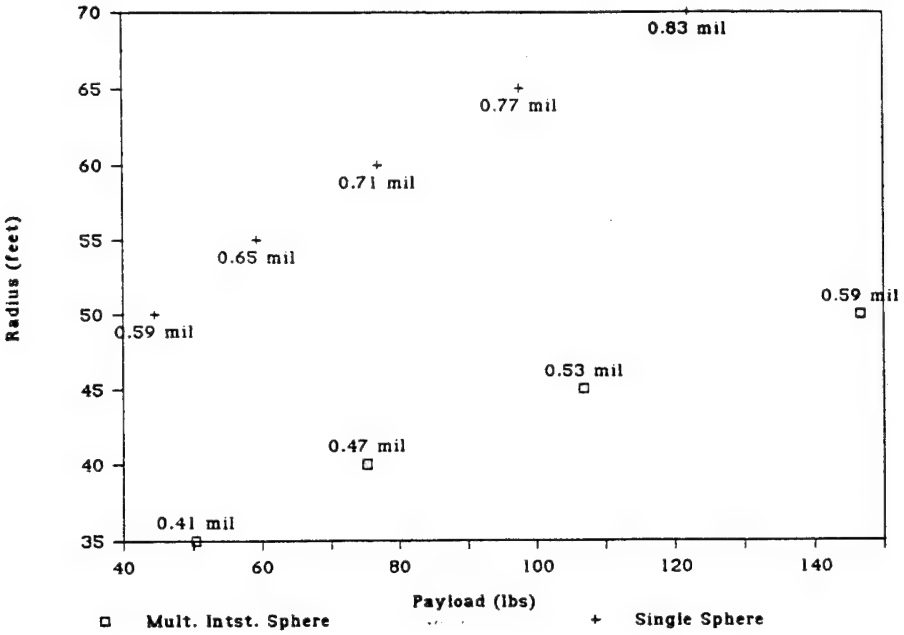

Figure 5-1. Balloon Weight Versus Payload Capacity for the Multiple Intersecting Sphere Balloon and the Single Sphere Balloon

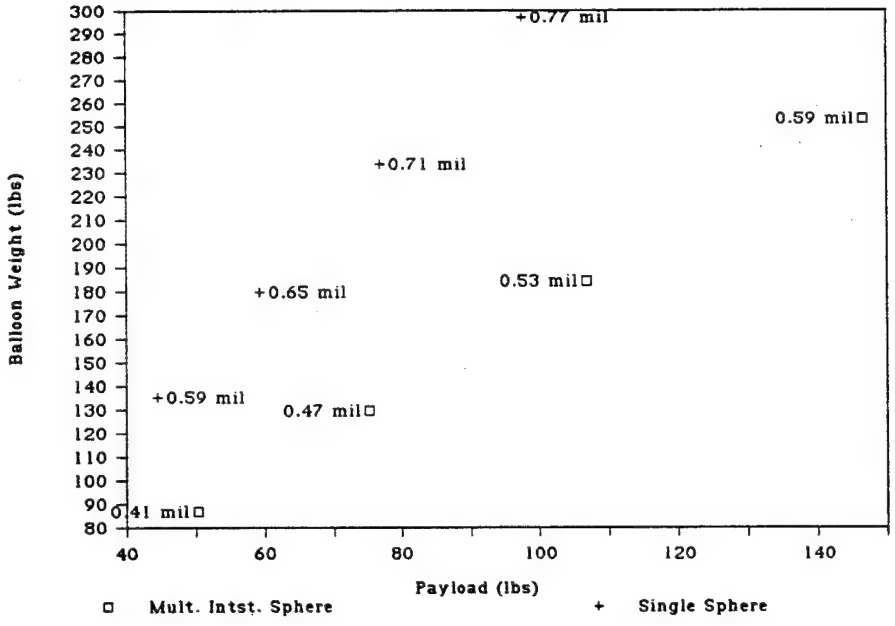

Figure 5-2. Balloon Radius Versus Payload Capacity for the Multiple Intersecting Sphere Balloon and the Single Sphere Balloon

Table 5-3. Balloon Weight and Payload Tradeoff						
	Triple Sphere			Single Sphere		
Radius (feet)	Balloon Weight (lbs)	Payload Capacity (lbs)	Thickness (mils)	Balloon Weight (lbs)	Payload Capacity (lbs)	Thickness (mils)
35	86.8	50.3	0.41	-	-	-
40	129.5	75.1	0.47	-	-	-
45	184.5	106.8	0.53	-	-	-
50	253.0	146.6	0.59	135.2	44.4	0.59
55	336.8	195.1	0.65	179.9	59.2	0.65
60	437.2	253.4	0.71	233.6	76.8	0.71
65	555.9	322.1	0.77	297	97.6	0.77
70	694.3	402.3	0.83	370.9	122	0.83

5.2.2 Calculations for Final Design

The final design was based on conditions corresponding to a winter flight from Sao Paulo, Brazil. As mentioned in Section 5.1, the worst nighttime conditions will occur on a cloudy night at 15° latitude with the gas temperature being -75°C and the air temperature being -26°C. The ambient nighttime air pressure under these conditions was determined using the ideal gas law:

$$P_a = \rho_a \frac{R_u}{M_a} T_{a,n} \qquad (5-1)$$

A minimum superpressure was specified to ensure that at the coldest temperatures, there would be enough superpressure left in the balloon for it to maintain its shape and, therefore, not change its volume significantly.

The minimum superpressure was added to the ambient nighttime air pressure to get the minimum absolute pressure of the gas inside the balloon. A superpressure corresponding to 1000 feet of helium was chosen as the minimum superpressure. Our FULSIZ natural shape balloon design program indicated that with this much superpressure, the shape was virtually spherical. This pressure head is converted into more common units by:

$$\Delta\rho = \rho_a \times (1 - M_g/M_a) \qquad (5-2)$$

$$= 0.0064389 kg/m^3 \times (1 - 4.0026/28.9644)$$

$$\Delta\rho = \rho_a \times (1 - M_g / M_a) \qquad (5-2)$$

$$= 0.0064389 kg/m^3 \times (1 - 4.0026/28.9644)$$

$$= 0.0055491 kg/m^3$$

$$\Delta P = \Delta\rho \times g \times h \qquad (5-3)$$

$$= 0.055491 kg/m^3 \times 9.81 m/s^2 \times 304.8 m$$

$$= 16.592 N/m^2$$

$$P_o = 0.16592 mbar \qquad (5-4)$$

The minimum gas pressure is then given by:

$$P_{g,n} = P_{a,n} + P_o \qquad (5-5)$$

Since the volume of the balloon is assumed constant and the mass of the gas inside the balloon should not change, its density is also a constant which can be determined from the ideal gas law.

The worst daytime condition will occur on a clear day at 30° latitude with the gas temperature being -21°C and the air temperature being -30°C. These temperatures result in a maximum pressure differential across the film of 1.53 mbar, according to Equation (3-14).

5.3 FINAL DESIGN

Using results from the design calculations, a series of balloon designs were generated. Table 5-4 shows the final designs for the single sphere balloon and MIS balloon with two through six spheres. The conditions for each design are assumed to be the following:

Final Design Conditions

$T_{g,n}$ = -75°C, Nighttime Gas Temperature

$T_{a,n}$ = -26°C, Nighttime Air Temperature

$T_{g,d}$ = -21°C, Daytime Gas Temperature

$T_{a,d}$ = -30°C, Daytime Air Temperature

P_o = 0.166 mbar, Minimum Superpressure

P	= 1.53 mbar, Maximum Superpressure
Number of Load Lines	= 8
Initial Angle of Load Lines	= 35° from Vertical

The load attachment design is as follows. The payload is to be suspended from Kevlar lines. Each load line extends from the payload over the top of the balloon where they cross, and back down to the payload. The load lines are not sealed to the balloon wall but are free to move along the balloon surface through small loops. The loops are sealed into the balloon at regular intervals. In this design, the balloon functions like a giant pulley, providing support perpendicular to the load line. The loops restrict the load lines' lateral movement, preventing the lines from tangling with each other.

This method of load attachment is desirable for two reasons. It does not create stress concentrations in the balloon wall, unlike some previous methods. Also, with this method, there is no need to increase the balloon wall thickness to support the meridional load.

Table 5-4. Final Designs

Number of Spheres	Radius (feet)	a/R	Volume (cu.ft.)	Surface Area (sq.ft.)	Required Thickness (mils)	Lift/Weight Ratio
1	53.8	0.00	652,000	36,400	0.72	1.30
2	41.1	0.60	521,00	34,000	0.55	1.41
3	35.7	0.57	481,000	34,300	0.48	1.46
4	32.6	0.57	477,000	36,200	0.43	1.47
5	30.1	0.55	453,000	36,400	0.40	1.49
6	28.5	0.56	462,000	38,800	0.38	1.49
Number of Spheres	Balloon Weight (lbs)	=	Film Weight (lbs)	Tape Weight (lbs)	Belt Weight (lbs)	Load Line Weight (lbs)
1	165	=	156.5	6.5	0.0	2.3
2	122	=	111.6	4.0	4.0	2.4
3	109	=	97.8	3.4	5.0	2.5
4	107	=	94.3	3.2	6.8	2.8
5	100	=	87.7	3.0	6.6	2.9
6	102	=	88.4	3.0	7.8	3.1

5.4 REFERENCES

5-1 Lenorvitz, J.M., "Soviets, U.S. Make Progress on Space Cooperation Talks," Aviation Week and Space Technology, Vol. 129, No. 5, 1 August 1988, pp. 42-43.

5-2 Tefft, J.D., "Nimbus - D/IRLS Superpressure Balloons in the Tropical Stratosphere", National Center for Atmospheric Research, Proceedings of the Sixth AFCRL Scientific Balloon Symposium, 27 October 1970.

6.0 MODEL TESTING

During the Phase I effort, initial tests were conducted to support the development of the tape and adhesive system used for joining the gores of the balloon. Initially, static tensile and creep tests were conducted using small film samples. These tests were followed by the fabrication and burst testing of cylinder balloons to assess seal strength and seal integrity. Once the tape and adhesive system was perfected, scale model spherical and double sphere MIS balloons were fabricated and burst tested. The description and results of these tests are given in this section.

6.1 TAPE AND ADHESIVE TESTING

Prior to fabrication of cylinders, development of the tape and adhesive system was completed and tested. A very convenient method was developed for making the tape in which sheets of Emblem® were coated on one side with adhesive and cut into strips. This section describes the method in detail.

A solution of 15 wt% of adhesive dissolved in m-propanol was used to prepare the adhesive tape. The 0.48 mil film was smoothed onto a glass plate and was coated with the solution using an adjustable coating knife (Pacific Scientific, Model AG-4304) set at various gaps. One-inch wide tapes with three different adhesive thicknesses were made. They were 0.5, 0.2, and 0.1 mils thick and were made with a gap setting of 10.0, 5.0, and 2.0 mils, respectively.

Several seals to the nylon film were made using the one-inch wide tapes. Two sections of film were butted together and the one-inch wide tape placed on top such that half the tape was on each side of the joint. Then the seal was made using a rotary heat sealer (Century, Model 70) at various temperatures. The sealed material was then turned over and another tape was applied in a similar manner.

One-inch wide strips of sealed material were cut using a razor blade and tested in an Instron tensile tester at -80°F with a four-inch jaw separation and a rate of separation of two inches/minute. These tests were conducted to determine the conditions under which good seals could be obtained. The test specimens were made with three different thicknesses of adhesive (0.5 mil, 0.2 mil, and 0.1 mil) and three seal temperatures (250°F, 300°F, and 340°F). For all specimens fabricated and tested, no failure occurred in the sealed region.

Samples of the seals were also evaluated for longer term shear resistance. One-inch wide specimens were hung with a 5.75 pound weight for a period totalling three weeks with no slippage occurring in the seal. The four-inch length had stretched initially to five inches, but there was no further change.

Based upon these tests, it was decided that a wide range of adhesive thicknesses and seal temperatures could be used for fabricating the balloons. This is important to note since it implies that tight tolerances will not be required in the seal fabrication process.

6.2 CYLINDER TESTS

Cylinders were used in the seal optimization tests because they are simple and quick to make. This is because they require straight seals. Also, they can be pressurized to failure to check the strength of the seals and material.

Cylinders were constructed by taking the 26 inch wide material and butt sealing the sides together. The tape was one-inch wide material and had 0.25 mils of adhesive. The tape was applied to both sides of the seal and the sealer temperature was 250°F. The cylinders were approximately three feet long. One end was sealed closed like the end of a pillow. The other end was securely clamped to a six-inch diameter end fitting. The circumference was measured during pressurization. The circumference varied only at the ends. Table 6-1 contains the data for four cylinder burst tests. The bursts occurred too quickly for the eye to see where the failure originated. The tear would propagate in a random direction. If it ran into a seal, the tear would then propagate along the seal, but not through the seal. In all cases, the seal remained intact, and there was no evidence of seal damage. The engineering hoop stress was based upon the relation:

$$\sigma_{hoop} = \frac{PR}{t} \qquad (6-1)$$

Table 6-1. Cylinder Pressurization Measurements

	Final Circumference (inches)	Hoop Strain (%)	Burst Pressure (inches H^2O)	Engineering Hoop Stress (psi)
Cylinder 1	30	15	56	17,400
Cylinder 2	34	31	56	17,400
Cylinder 3	32	23	49	15,200
Cylinder 4	33	27	56	17,400

6.3 SINGLE SPHERE TESTING

To demonstrate that it was feasible to construct a sphere and that it could sustain design stresses, several three foot diameter spheres were made using 0.48 mil Emblem® film, which was the only thickness of material available at this time. For large quantities, it should be possible to get the film in any desired thickness. The sphere was constructed of eight gores. A glass template of the gore pattern was purchased and each gore was cut from the material with a razor blade. The gores were butt sealed to each other using one-inch wide tape applied to the inside and outside of the seal. At one end of the sphere, where the tips of the gores met, an end cap of the same material was sealed in. At the other end, an aluminum flange with a rubber gasket was used to close off the end. A connection for filling the balloon with gas was provided in this end fitting. The first sphere was pressurized to failure at room temperature. It burst at a calculated stress of 12,900 psi. This value was lower than anticipated, which was probably due to defects in the seals.

Four spheres were later pressurized to failure in the cold chamber located at the National Scientific Balloon Facility in Palestine, Texas. The Bemco chamber was cooled by passing liquid nitrogen through cooling coil panels inside the chamber. It took between 15 and 30 minutes to cool the chamber for each test. Compressed air was used to pressurize the balloon. The supply tank and water column manometer were outside the chamber. Air supply for inflation was controlled by a manual valve. The supply line passed through a hole in the chamber wall and was run along the chamber floor to a wooden stand with the connection fitting. The gas fitting was connected to the base fitting on each balloon. The balloon was partially inflated at room temperature and placed inside the chamber (Figure 6-1). Thermistors were taped to the balloon wall to monitor the film temperature. The door was closed and the temperature in the chamber was lowered. When the desired temperature was reached, the balloon was slowly pressurized (over a period averaging ten minutes) until it burst.

Table 6-2 lists the temperature of the balloon wall, the pressure at which it burst, and the engineering stress at failure, assuming the stress was equal to PR/2t. The second sphere failed at a low stress level. During its fabrication and leak testing, a small hole was accidently made in a gore. It was repaired with a piece of adhesive tape. In the cold box test, it was this gore which failed.

In general, it was not possible to observe where a failure began. A tear would open up the material and propagate in two directions. Typically, the tear would run up to a seal, then turn and continue tearing adjacent to the seal. It would run up to the end cap of the sphere, tear around the edge of the end cap, through some seals, and then continue tearing away from the end cap, running along another seal.

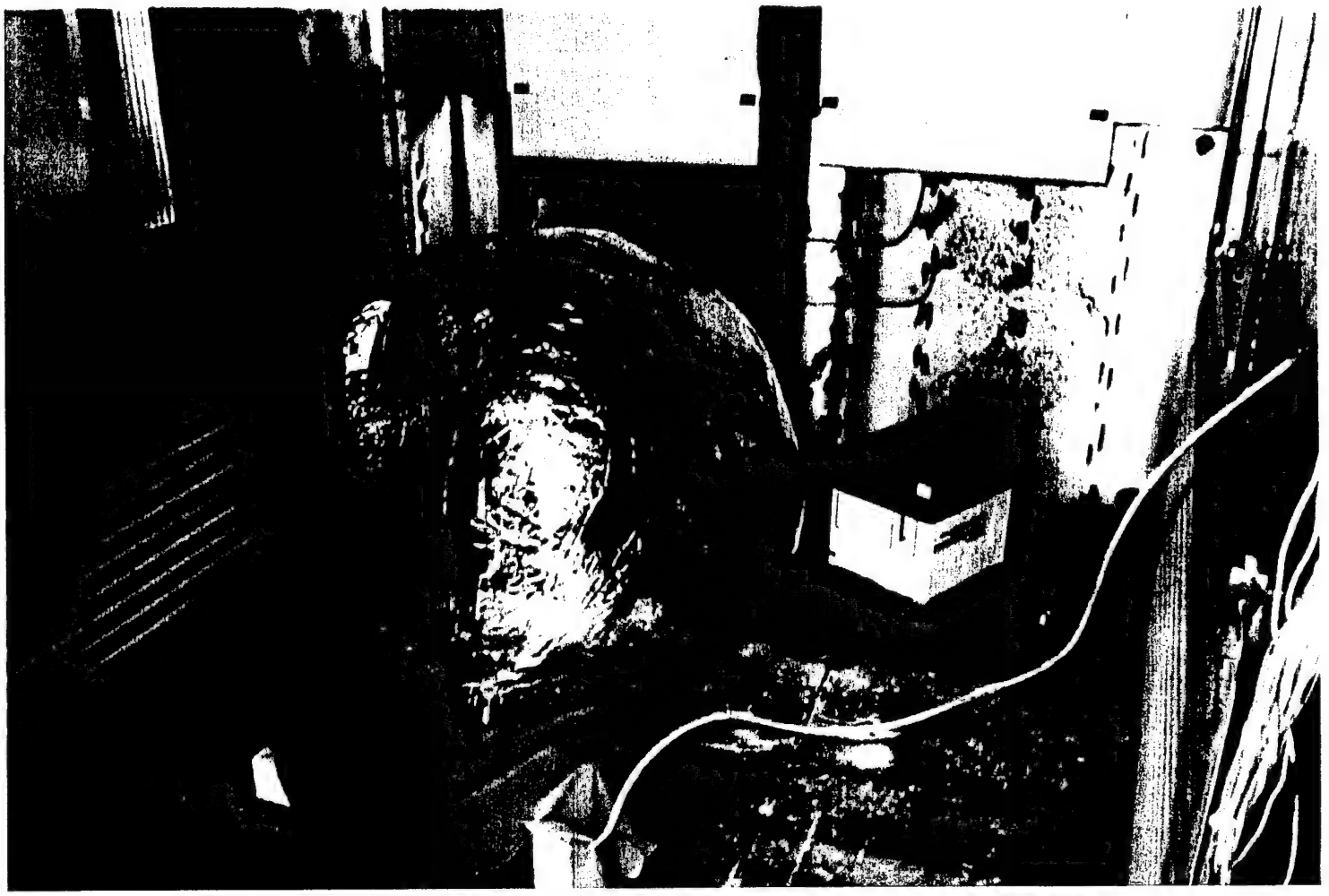

Figure 6-1. Partially Inflated Spherical Balloon Located in Cold Box Prior to Test

Table 6-2. Spherical Balloon Cold Box Measurements			
	Temperature (°C)	Gage Pressure (inches H^2O)	Engineering Biaxial Stress (psi)
Sphere 1	-31	27	18,300
Sphere 2	-41	12	8,100
Sphere 3	-38	30	20,300
Sphere 4	-20	24	16,300

6.4 MIS BALLOON TESTING

A double sphere MIS balloon model was constructed (Figure 6-2). Each spherical section had an 18-inch radius of curvature. The belt for this model balloon consisted of many layers of the same adhesive tape used for sealing the gores together. Since the longest piece of tape that could be readily made was six feet, the designed circumference of the belt was chosen as 5.5 feet and the distance between the spheres was chosen accordingly. The resulting parameters of the model balloon are calculated below:

$$R_b = \frac{66"}{2\pi} = 10.5" \tag{6-2}$$

$$\theta = \sin^{-1}\left(\frac{R_b}{R}\right) = 35.70° \tag{6-3}$$

Since

$$\sigma = \frac{\Delta P R}{2t} \tag{6-4}$$

$$\Delta P R = 2t\sigma \tag{6-5}$$

Substituting into Equation (3-22) to get the belt strength:

$$H = 2t\sigma \cos\theta r_b \tag{6-6}$$

$$= 2 \times .00048" \times 10,000 p.s.i. \times \cos 35.70 \times 10.5"$$

$$= 81.9 pounds force$$

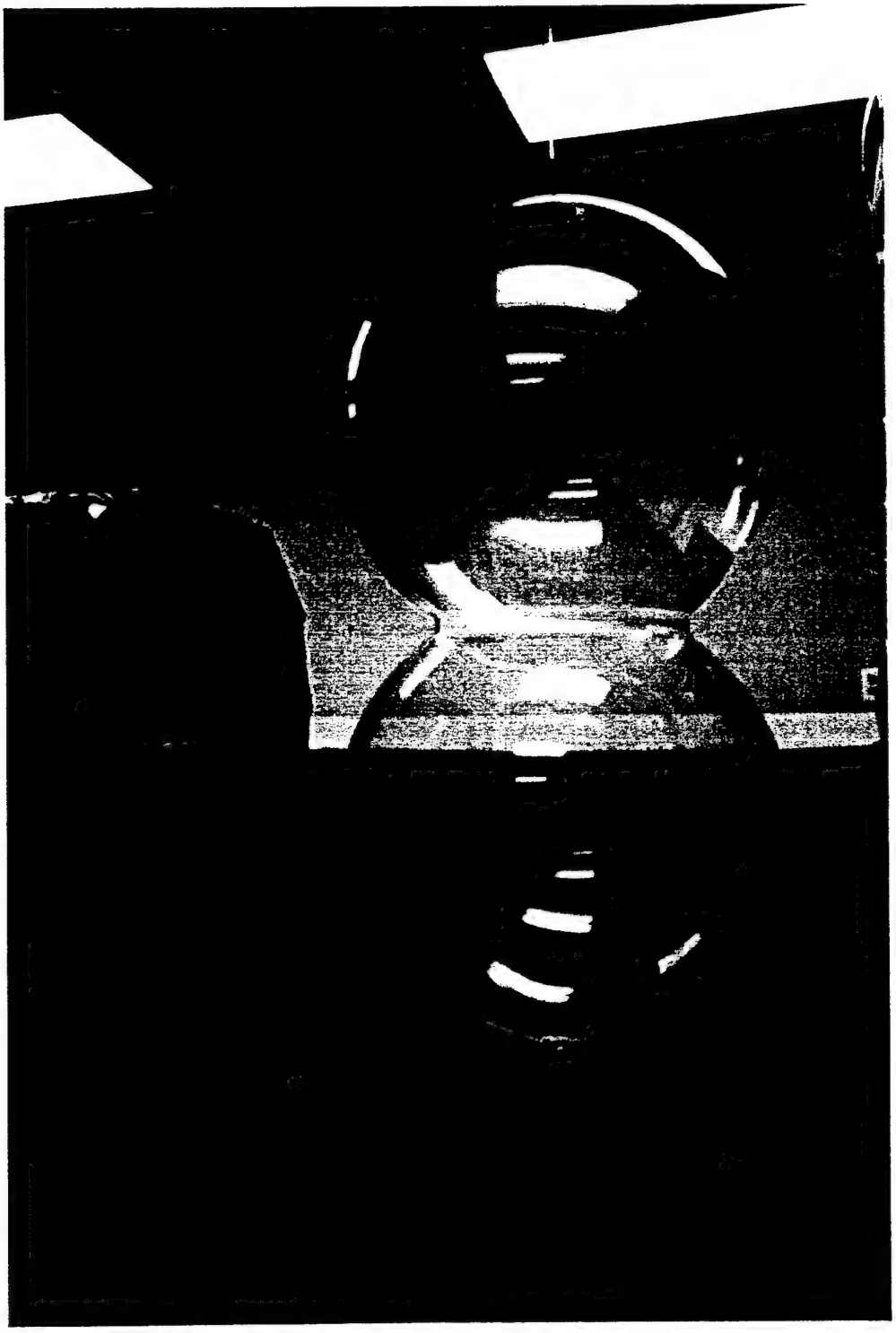

Figure 6-2. Double Sphere MIS Balloon Model

For a design stress of 10,000 psi, the cross-sectional area required was 0.0082 square inches. The belt was selected to be two inches wide so the required thickness was 4.1 mils. The actual belt consisted of nine layers of the 0.48 mil tape.

This MIS balloon was pressure tested at room temperature since it had not been fabricated at the time that the cold chamber was available. As the pressure was slowly increased, the belted region deformed from its cylindrical band shape to a shape where the edges of the belt were pushed outward, giving the belt a saddle-type shape. The balloon was pressurized to its design stress of, 10,000 psi and soon thereafter, a small hole opened up adjacent to the belt and next to a gore seal. The hole was a tear about one-inch long. It had been thought that a failure would appear in this region. It was observed as the balloon was being slightly pressurized that this region appeared to have the fewest wrinkles in the film. Reinforcement of this region will be addressed in the Phase II study.

7.0 SUMMARY AND CONCLUSIONS

During the Phase I effort, a new film was identified for use in the fabrication of superpressure balloons. This film, a recently developed biaxially oriented nylon 6, is trade named Emblem®. By virtue of its orientation, it displays very high strength properties at all temperatures. A major advantage is that unlike Mylar®, it does not suffer from flex cracking which causes small pinhole leaks. A heat activated adhesive was also identified which results in strong butt seals of the film.

A thermal analysis was conducted to determine the variations in day to night temperatures of the balloon gas at float. The resulting predictions for temperature ranges and, hence, internal pressure ranges in superpressure balloons at float were greater than expected. If these results are found to be accurate in Phase II, balloons will have to be designed for slightly higher temperature ranges than those used in previous designs.

A superpressure balloon design effort resulted in the identification of a relatively new concept named the multiple intersecting sphere (MIS) design. This concept, having the shape of two or more intersecting spheres, displays the advantage of the low film stresses inherent in the spherical shape with a reduction in required balloon diameter. Significant reductions in balloon weight were noted for a three or four sphere design as opposed to that of a single sphere. A belt design was developed for reinforcing the region formed by the intersection of the spheres and a harness system was identified.

Both room temperature and cold box tests were conducted of model balloons having three-foot diameters. Four spherical balloons were burst tested in a cold box at temperatures between -41° and -20°C. Discounting the premature failure from a manufacturing defect, the average burst pressure recorded for these tests corresponded to a film stress 83 percent greater than our current design specification. A single MIS balloon was burst tested at room temperature where the film strength is half that expected at the colder temperatures. Even so, film stresses exceeded the design stress of 10,000 psi at the time of burst.

The results of this Phase I effort clearly demonstrated the technical feasibility of developing a reliable superpressure balloon platform capable of supporting 50 pounds at 120,000 feet for extended periods. There were no insurmountable technical obstacles identified in Phase I. The Emblem® film is a dramatic improvement over films used for this purpose in past studies. (The major obstacle overcome was the susceptibility of prior films to pinholes which limits balloon life.) The MIS shape also promises to minimize balloon size and weight. In order to bring this system to the point of commercial and military application, a Phase II study is needed to address the following areas:

(1) Further characterization of the Emblem® film.

(2) Improved analysis of the thermal extremes to be expected by a balloon at float for long durations.

(3) Automated balloon fabrication technique development.

(4) Film and seal quality control method development.

(5) Designs for film reinforcement around the seals, belts, and support lines.

(6) Ground tests and flight tests of larger models of an MIS balloon.

APPENDIX A

DEFINITION OF SYMBOLS

DEFINITION OF SYMBOLS

Thermal Model

Symbol	Definition
G	Solar constant
α_g	Solar absorptivity of gas
r_e	Earth albedo reflectance
CH_{gw}	Convection coefficient between gas and wall
T_g	Temperature of gas
T_w	Temperature of wall
σ	Stefan-Boltzman constant
α_w	Solar absorptivity of wall
CH_{wa}	Convection coefficient between wall and air
T_a	Ambient air temperature
ϵ_{wir}	Wall IR emissivity
T_{BB}	Blackball temperature
ϵ_g	IR emissivity of gas
r_{wir}	IR reflectivity of wall
τ_{wir}	IR transmissivity of wall
τ_{wsol}	Solar transmissivity of wall
r_{wsol}	Solar reflectivity of wall
ϵ_{gw}	Effective coefficient of infrared interchange between balloon wall and gas
ϵ_{geff}	Effective coefficient of emissivity of the balloon gas
ϵ_{weff}	Effective coefficient of emissivity of the balloon wall
α_{geff}	Effective coefficient of absorptivity of the balloon gas
α_{weff}	Effective coefficient of absorptivity of the balloon wall

Mechanical Model

Symbol	Definition
$P_{a,d}$	Daytime air pressure
$P_{a,n}$	Nighttime air pressure
$P_{g,d}$	Daytime gas pressure
$P_{g,n}$	Nighttime gas pressure
P_o	Minimum gas superpressure
$T_{a,d}$	Daytime air temperature
$T_{a,n}$	Nighttime air temperature
$T_{g,d}$	Daytime gas temperature
$T_{g,n}$	Nighttime gas temperature
ρ_a	Air density
ρ_g	Gas density
R_u	Universal gas constant
M	Molecular weight
R	Balloon radius
α	Half the distance between the centers of intersecting spheres
Θ	The angle at which the intersecting spheres meet the horizontal plane
r_b	Belt radius
γ	Initial angle the load lines make with the vertical axis
t	Film thickness

APPENDIX B

DERIVATION OF MAXIMUM DAYTIME PRESSURE DIFFERENTIAL

DERIVATION OF MAXIMUM DAYTIME PRESSURE DIFFERENTIAL

This appendix derives the equations for calculating the maximum pressure differential between the lifting gas inside the superpressure balloon and the surrounding air. This appendix was called out in Section 3.3 of the report. This derivation assumes that the balloon volume does not change and that a minimum gage pressure of P_o must be maintained inside the balloon in order to maintain its shape. Inputs which drive the equation are the most severe combination of nighttime and daytime temperatures of the surrounding air and of the lifting gas. The superpressure balloon is designed to fly a constant density altitude profile, so ρ_a is a known constant. Since the mass of gas in the balloon, and the volume of the balloon are assumed to be constant, the gas density is also assumed to be constant.

Assuming the atmosphere to be an ideal gas, the pressure at night is given by:

$$P_{a,n} = \rho_a \frac{R_u}{M_a} T_{a,n} \qquad (B-1)$$

By definition, the minimum gage pressure of the lifting gas is:

$$P_{g,n} = P_{a,n} + P_o \qquad (B-2)$$

Substituting Equation (B-1) into (B-2) yields:

$$P_{g,n} = \rho_a \frac{R_u}{M_a} T_{a,n} + P_o \qquad (B-3)$$

Assuming the lifting gas to be an ideal gas, the density is given by:

$$\rho_g = \frac{M_g}{R_u T_{g,n}} P_{g,n} \qquad (B-4)$$

Substituting Equation (B-3) into Equation (B-4) yields:

$$\rho_g = \frac{M_g}{R_u T_{g,n}}\left[\rho_a \frac{R_u}{M_a} T_{a,n} + P_o\right] \qquad (B-5)$$

The maximum superpressure will occur during the day and is defined as:

$$\Delta P = P_{g,d} - P_{a,d} \qquad (B-6)$$

Assuming both gases to obey the ideal gas law yields:

$$\Delta P = \left(\frac{R_u}{M_g}\right)\rho_g T_{g,d} - \left(\frac{R_u}{M_a}\right)\rho_a T_{a,d} \qquad (B-7)$$

Substituting Equation (B-5) into Equation (B-7) yields:

$$\Delta P = \frac{R_u}{M_g}\left[\frac{M_g}{R_u}\frac{1}{T_{g,n}}\left(\rho_a \frac{R_u}{M_a} T_{a,n} + P_o\right)\right] T_{g,d} - \left(\frac{R_u}{M_a}\right)\rho_a T_{a,d}$$

Which may be simplified as:

$$\Delta P = \frac{T_{g,d}}{T_{g,n}}\left(\frac{\rho_a R_u}{M_a} T_{a,n} + P_o\right) - \left(\frac{\rho_a R_u}{M_a}\right) T_{a,d}$$

Which may be rearranged to yield:

$$\Delta P = \frac{\rho_a R_u}{M_a}\left[\frac{T_{g,d}}{T_{g,n}} T_{a,n} - T_{a,d} + \frac{T_{g,d}}{T_{g,n}}\frac{M_a}{\rho_a R_u} P_o\right] \qquad (B-8)$$

APPENDIX C

VOLUME AND SURFACE AREAS OF TRUNCATED HEMISPHERES

VOLUME AND SURFACE AREAS OF TRUNCATED HEMISPHERES

This appendix derives the equations used to calculate the volume and surface area of the Multiple Intersecting Sphere (MIS) balloon. The MIS balloon's geometry consists of portions of spheres (Figure C-1). The top and bottom are hemispheres, but the regions of the spheres which intersect have geometries resembling truncated hemispheres.

The following derivations for the volume and the surface area of truncated hemispheres refer to the coordinate system shown in Figure C-2.

$$Volume = \int_0^a \pi x^2 dy, \; x^2 = R^2 - y^2 \qquad (C-1)$$

$$= \int_0^a \pi (R^2 - y^2) dy$$

$$= \pi R^2 y \Big|_0^a - 1/3 \pi y^3 \Big|_0^a$$

$$= \pi R^2 a - 1/3 \pi a^3$$

$$Surface\,Area = \int_0^a 2\pi f(y) \sqrt{1 + [f'(y)]^2}\, dy \qquad (C-2)$$

$$f(y) = x = (R^2 - y^2)^{1/2} \qquad (C-3)$$

$$f'(y) = \frac{1}{2}(R^2 - y^2)^{-1/2}(-2y) \qquad (C-4)$$

$$= -\frac{y}{(R^2 - y^2)^{1/2}}$$

$$[f'(y)]^2 = \frac{y^2}{R^2 - y^2} \qquad (C-5)$$

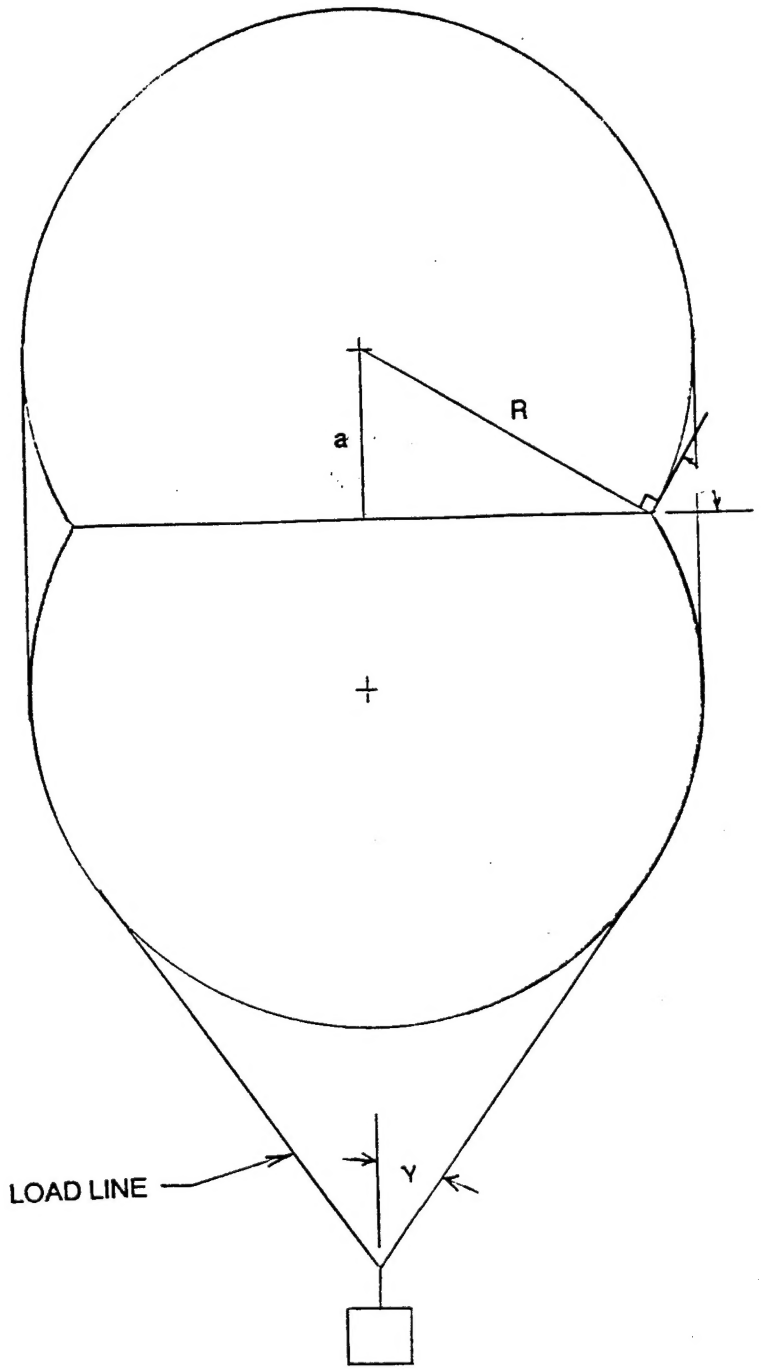

Figure C-1. MIS Balloon

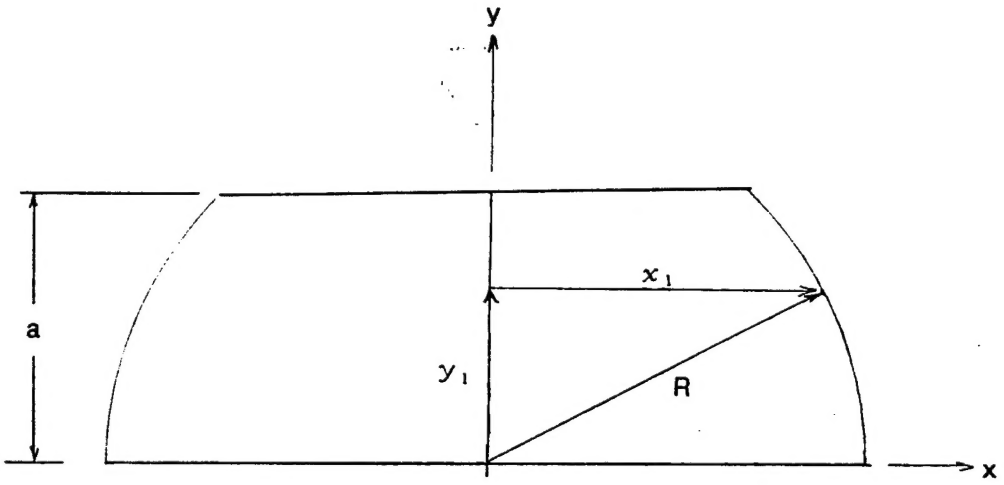

Figure C-2. Truncated Hemisphere

Substituting into Equation (C-2):

$$Surface\,Area = 2\pi\int_0^a (R^2 - y^2)^{1/2}\left[1 + \frac{y^2}{R^2 - y^2}\right]^{1/2} dy$$

$$= 2\pi\int_0^a [R^2 - y^2 + y^2]^{1/2} dy$$

$$= 2\pi\int_0^a R\,dy$$

$$= 2\pi R a$$

A MIS balloon with N-spheres has two complete hemispheres at the top and bottom and (N-1) belts. Each belt has two truncated hemispheres attached to it. Therefore, the volume for an N-sphere MIS balloon is:

$$V_n = 4/3 \times \pi \times R^3 + (N-1) \times 2 \times \pi \times (R^2 \times a - 1/3 \times a^3) \qquad (C-6)$$

and its surface area is:

$$SA_n = 4 \times \pi \times R^2 + (N-1) \times 4 \times \pi \times R \times a \qquad (C-7)$$